

# Oscillatory Instabilities and Dynamics of Multi-Spike Patterns for the One-Dimensional Gray-Scott Model

Wan Chen\*, Michael J. Ward†

## Abstract

The dynamics and oscillatory instabilities of multi-spike solutions to the one-dimensional Gray-Scott reaction-diffusion system on a finite domain are studied in a particular parameter regime. In this parameter regime, a formal singular perturbation method is used to derive a novel ODE-PDE Stefan problem, which determines the dynamics of a collection of spikes for a multi-spike pattern. This Stefan problem has moving Dirac source terms concentrated at the spike locations. For a certain subrange of the parameters, this Stefan problem is quasi-steady and an explicit set of differential-algebraic equations characterizing the spike dynamics can be derived and analyzed. By analyzing a nonlocal eigenvalue problem, it is found that this multi-spike quasi-equilibrium solution can undergo a Hopf bifurcation leading to oscillations in the spike amplitudes on an  $O(1)$  time-scale. In another subrange of the parameters, the spike motion is not quasi-steady and the full Stefan problem is solved numerically by using an appropriate discretization of the Dirac source terms. In this regime it is shown from full numerical computations and from a linearization of the Stefan problem that the spikes can undergo a drift instability arising from a Hopf bifurcation. This instability leads to a time-dependent oscillatory behavior in the spike locations.

## 1 Introduction

The Gray-Scott (GS) system models an irreversible reaction in a gel reactor where the reactor is maintained in contact with a reservoir of one of the two chemical species. In one spatial dimension, it can be written in dimensionless form in the singularly perturbed limit as (cf. [23], [17])

$$v_t = \epsilon^2 v_{xx} - v + \mathcal{A}uv^2, \quad v_x = 0, \quad x = \pm 1, \quad (1.1a)$$

$$\tau u_t = Du_{xx} + (1 - u) - \epsilon^{-1}uv^2, \quad u_x = 0, \quad x = \pm 1. \quad (1.1b)$$

Here  $\mathcal{A} > 0$  is the feed-rate parameter,  $\tau > 0$  is the reaction-time parameter,  $D > 0$  with  $D = O(1)$ , and  $\epsilon > 0$  with  $\epsilon \ll 1$ .

The pioneering numerical study of [29] for the GS model in a two-dimensional spatial domain showed that localized spike solutions for this model can exhibit a remarkably diverse range of qualitative behaviors including, self-replication behavior of spikes, breathing instabilities of spikes, spike annihilation behavior due to over-crowding etc. This numerical study has stimulated much theoretical work to analyze and classify the full range of dynamical behavior and instabilities of spike solutions for the more tractable

---

\*Department of Mathematics, University of British Columbia, Vancouver, Canada V6T 1Z2

†Department of Mathematics, University of British Columbia, Vancouver, Canada V6T 1Z2, (corresponding author)

one-dimensional GS model (1.1) in the limit  $\varepsilon \rightarrow 0$ . These studies include self-replication behavior in the regime  $D = O(\varepsilon^2)$  (cf. [26], [33]) and in the regime  $D = O(1)$  (cf. [30], [4], [23], [18]), spatial temporal chaos for  $D = O(\varepsilon^2)$  (cf. [27]), the existence and stability of equilibrium spike patterns for  $D = O(1)$  (cf. [4], [5], [22], [21], [17], [19]), and the slow dynamics of quasi-equilibrium spike patterns (cf. [2], [3], [31]).

More generally, there has been several formal asymptotic studies of spike motion for two-component singularly perturbed reaction-diffusion systems in the limit of small diffusivity of only one of the two species. These include, two-spike dynamics for the GS model on the infinite domain (cf. [2], [3]),  $k$ -spike dynamics with  $k \geq 1$  for an elliptic-parabolic limit of the Gierer-Meinhardt (GM) model (cf. [12]), two-spike dynamics for a class of problems including a regularized GM model on the infinite line (cf. [6]), and two-spike dynamics for the GM model and for the GS model in the low feed-rate regime  $\mathcal{A} = O(1)$  on a finite domain (cf. [31]). Recently, in [7] a renormalization method was used to rigorously analyze two-spike dynamics for a regularized GM model on the infinite line.

The goal of this paper is to analyze the dynamics and oscillatory instabilities of multi-spike solutions to the GS model (1.1) in the intermediate regime  $O(1) \ll \mathcal{A} \ll O(\varepsilon^{-1/2})$  of the feed-rate parameter  $\mathcal{A}$ . The novelty and significance of this intermediate parameter regime is that, in terms of the reaction-time parameter  $\tau$ , there are two distinct subregimes in  $\mathcal{A}$  where qualitatively different types of spike dynamics and instabilities occur. In addition, in the intermediate parameter regime a formal singular perturbation analysis, as summarized in Principal Result 2.1, reveals that an ODE-PDE coupled Stefan-type problem with moving Dirac source terms determines the time-dependent locations of the spike trajectories. The derivation and study of this Stefan problem is a new result for spike dynamics in the GS model. Finally, in contrast to previous studies, our study is not limited to the special case of two-spike dynamics. In our analysis we can readily treat an arbitrary number of spikes for (1.1) in the regime  $O(1) \ll \mathcal{A} \ll O(\varepsilon^{-1/2})$ .

In the subregime  $O(1) \ll \mathcal{A} \ll O(\varepsilon^{-1/3})$  with  $\tau \ll O(\varepsilon^{-2}\mathcal{A}^{-2})$ , the Stefan problem is quasi-steady and we derive an explicit differential-algebraic (DAE) system for the spike trajectories. The result is given in Principal Result 2.2. For the case of a two-spike evolution, in Fig. 1 we illustrate our result by plotting the quasi-equilibrium solution for  $u$  and  $v$  together with the spike trajectories for a particular set of the parameter values. In this subregime, where the speed of the spikes is  $O(\varepsilon^2\mathcal{A}^2) \ll 1$ , we show from the analysis of a nonlocal eigenvalue problem (NLEP) that the instantaneous quasi-equilibrium spike solution first loses its stability to a Hopf bifurcation in the spike amplitudes when  $\tau = \tau_H = O(\mathcal{A}^4)$ . This bifurcation leads to oscillations on an  $O(1)$  time scale in the amplitudes of the spikes. Our stability results are given in Principal Results 3.1 and 3.2. These NLEP stability results are the first such results for multi-spike quasi-equilibrium patterns for the GS model on a finite domain with an arbitrary number of spikes. An important remark is that our NLEP stability analysis in the intermediate regime for a multi-spike pattern with  $O(1)$  inter-spike distances can be reduced to the study of a *single* NLEP problem. This feature, which greatly simplifies the stability analysis, is in distinct contrast to the stability analysis of [31] and [17] for the GS model in the low feed-rate regime  $\mathcal{A} = O(1)$ , and for the corresponding Gierer-Meinhardt model (see [12], [7], [34]), where  $k$ -distinct NLEP problems govern the stability of  $k$ -spike patterns.

Next, we study spike dynamics in the subregime  $O(\varepsilon^{-1/3}) \ll \mathcal{A} \ll O(\varepsilon^{-1/2})$  with  $\tau = \tau_0\varepsilon^{-2}\mathcal{A}^{-2}$ , for some  $O(1)$  bifurcation parameter  $\tau_0$ . In this regime, the time-dependent spike locations are determined

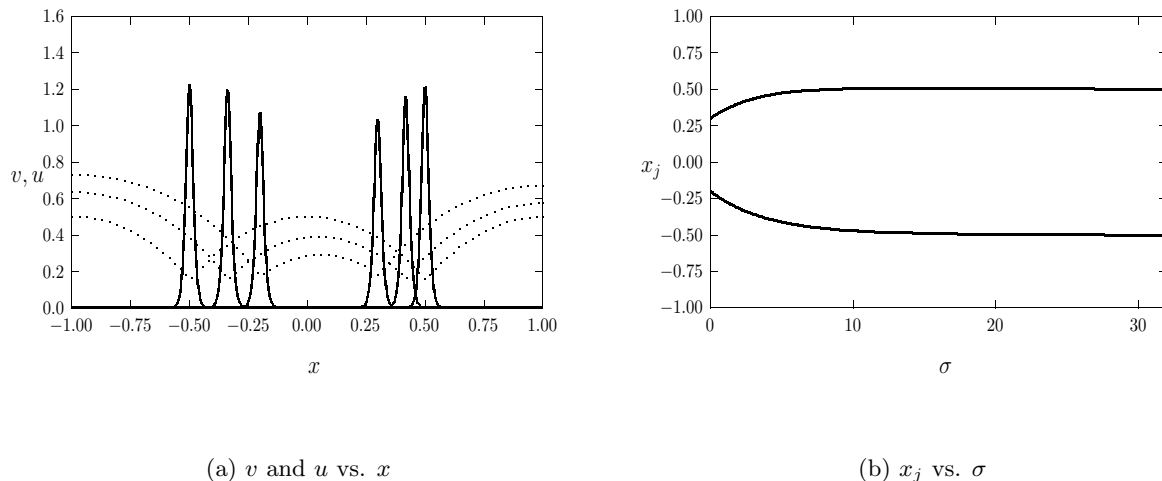


Figure 1: Slow dynamics, for  $\varepsilon = 0.01$ ,  $\mathcal{A} = 8$ , and  $D = 0.2$ , of a two-spike quasi-equilibrium solution with  $x_1(0) = -0.2$  and  $x_2(0) = 0.3$ . Left figure: plot of  $v$  (solid curves) and  $u$  (dotted curves) versus  $x$  at  $\sigma = 0$ ,  $\sigma = 2.5$ , and  $\sigma = 30$ . Right figure: plot of  $x_j$  versus  $\sigma = \varepsilon^2 \mathcal{A}^2 t$ . As the slow time  $\sigma$  increases, the spike layers approach their steady state limits at  $x = \pm 1/2$ .

from the full numerical solution of a Stefan-type problem with moving Dirac source terms concentrated at the unknown spike locations. Similar moving boundary problems arise in the study of the immersed boundary method (see [1] and [32]). The numerical method that we use for our Stefan problem relies on the approach of [32] involving a high-order spatial discretization of singular Dirac source terms. Such high spatial accuracy is needed in our problem in order to accurately calculate the average flux for  $u$  at each source point, which determines the speed of each spike. An explicit time integration scheme is then used to advance the spike trajectories each time step. With this numerical approach we compute large-scale time-dependent oscillatory motion in the spike locations when the reaction-time parameter  $\tau_0$  exceeds some critical bifurcation value. Although the overall scheme has a high spatial order of accuracy, the explicit time integration step renders our numerical scheme not particularly suitable for studying large-scale drift instabilities over very long-time intervals.

By linearizing the Stefan problem around an equilibrium spike solution, we analytically calculate a critical value of  $\tau_0$  at which the equilibrium solution becomes unstable to small-scale oscillations in the equilibrium spike location. This bifurcation value of  $\tau_0$  gives the threshold value for an oscillatory drift instability. The result is given in Proposition 4.1. This bifurcation result, based on a linearization of the Stefan problem, agrees with the result derived in [19] using the singular limit eigenvalue problem (SLEP) method of [24].

The SLEP method has been extensively used to study similar oscillatory drift instabilities that lead to the destabilization of equilibrium transition layer solutions for Fitzhugh-Nagumo type systems (cf. [25], [11]). With this method, Hopf bifurcation values for the onset of the instability can be calculated and the dominant translation instability, either zigzag or breather, can be identified (cf. [25]). For spatially

extended systems on the infinite line, it is then often possible to perform a centre manifold reduction, valid near the Hopf bifurcation point, to develop a weakly nonlinear normal form theory for large-scale oscillatory drift instabilities (see [9], [8] and the references therein). In contrast to this normal form theory, we emphasize that our Stefan problem with moving sources provides a description of large-scale oscillatory drift instabilities for values of  $\tau_0$  not necessarily close to the Hopf bifurcation point.

Similar Stefan problems with moving Dirac source terms have appeared in a few other contexts. In particular, such a problem determines a flame-front interface in the thin reaction zone limit of a certain PDE model of solid fuel combustion on the infinite line (cf. [28]). By using the heat kernel, this Stefan problem was reformulated in [28] into a nonlinear integrodifferential equation for the moving flame-front interface. By solving this integrodifferential equation numerically, a periodic doubling cascade and highly irregular relaxation oscillations of the flame-front interface were computed in [28]. For a related Stefan problem arising from solid combustion theory, a three-term Galerkin type-truncation was used in [10] to qualitatively approximate the Stefan problem by a more tractable finite dimensional dynamical system, which can then be readily analyzed. Finally, we remark that in [14] a time-dependent moving source with prescribed speed was shown to prevent blowup behavior for a certain class of nonlinear heat equation.

An outline of this paper is as follows. In §2 we derive the Stefan problem governing spike dynamics in the intermediate regime  $O(1) \ll \mathcal{A} \ll O(\varepsilon^{-1/2})$ . In §2.1 we analyze the quasi-steady limit of this problem. In §3 we analyze the stability of the quasi-equilibrium spike patterns of §2.1 in the subregime  $O(1) \ll \mathcal{A} \ll O(\varepsilon^{-1/3})$ . In §4 we compute numerical solutions to the Stefan problem showing large-scale oscillatory drift instabilities in the subregime  $O(\varepsilon^{-1/3}) \ll \mathcal{A} \ll O(\varepsilon^{-1/2})$ . In addition, a critical value of  $\tau_0$  for the onset of this instability is determined analytically. Concluding remarks are made in §5.

## 2 The Dynamics of $k$ -Spike Quasi-Equilibria: A Stefan Problem

In this section we first derive the ODE-PDE Stefan problem that determines the time-dependent trajectories of the spike locations for (1.1) in the intermediate regime  $O(1) \ll \mathcal{A} \ll O(\varepsilon^{-1/2})$ .

To do so we first motivate the scalings of  $u$ ,  $v$ , and the slow time that are needed for describing spike dynamics when  $O(1) \ll \mathcal{A} \ll O(\varepsilon^{-1/2})$ . In the inner region, we introduce a scaling such that  $\mathcal{A}uv = O(1)$ , with  $v = O(\mathcal{A})$  as suggested by the equilibrium theory of Section 4 of [17]. We also introduce the slow time  $\sigma = \sigma_0 t$ , with  $\sigma_0 \ll 1$ . With  $v = \mathcal{A}v_j$ ,  $u = u_j/\mathcal{A}^2$ , and  $y = \varepsilon^{-1} [x - x_j(\sigma)]$ , where  $\sigma = \sigma_0 t$ , (1.1) becomes

$$-\varepsilon^{-1}\sigma_0 \frac{dx_j}{d\sigma} v_j' = v_j'' - v_j + u_j v_j^2, \quad -\frac{\sigma_0 \tau}{\mathcal{A}^2} \left( \frac{dx_j}{d\sigma} \right) u_j' = \frac{D}{\varepsilon \mathcal{A}^2} u_j'' + \varepsilon \left( 1 - \frac{u_j}{\mathcal{A}^2} \right) - u_j v_j^2, \quad (2.1)$$

where the primes on  $u_j$  and  $v_j$  indicate derivatives in  $y$ . The equation for  $u_j$  suggests that  $u_j = u_{j0} + O(\varepsilon \mathcal{A}^2)$ , where  $u_{j0}$  is a constant. This enforces from the  $v_j$  equation that  $v_j = v_{j0} + O(\varepsilon \mathcal{A}^2)$ , and  $\sigma_0 = \varepsilon^2 \mathcal{A}^2$ . Since  $u_j$  is independent of  $y$  to leading order, the left-hand side of the  $u_j$  equation can be neglected only when  $\sigma_0 \tau \varepsilon \mathcal{A}^2 / \mathcal{A}^2 \ll 1$ . With  $\sigma_0 = \varepsilon^2 \mathcal{A}^2$ , this condition is satisfied only when  $\tau \varepsilon^3 \mathcal{A}^2 \ll 1$ .

This simple scaling argument suggests that we expand the solution in the  $j^{\text{th}}$  inner region as

$$u = \frac{1}{\mathcal{A}^2} [u_{0j} + \varepsilon \mathcal{A}^2 u_{1j} + \dots], \quad v = \mathcal{A} [v_{0j} + \varepsilon \mathcal{A}^2 v_{1j} + \dots], \quad (2.2a)$$

where  $u_{mj} = u_{mj}(y, \sigma)$  and  $v_{mj}(y, \sigma)$  depend on the inner variable  $y$  and the slow time  $\sigma$  defined by

$$y \equiv \varepsilon^{-1} [x - x_j(\sigma)] , \quad \sigma \equiv \varepsilon^2 \mathcal{A}^2 t . \quad (2.2b)$$

Upon substituting (2.2) into (1.1), and assuming that  $\tau \varepsilon^3 \mathcal{A}^2 \ll 1$ , we obtain the leading-order problem

$$v''_{0j} - v_{0j} + u_{0j} v_{0j}^2 = 0 , \quad u''_{0j} = 0 , \quad -\infty < y < \infty . \quad (2.3)$$

At next order we obtain

$$v''_{1j} - v_{1j} + 2u_{0j} v_{0j} v_{1j} = -u_{1j} v_{0j}^2 - x'_j v'_{0j} , \quad Du''_{1j} = u_{0j} v_{0j}^2 , \quad -\infty < y < \infty . \quad (2.4)$$

From (2.3) we take  $u_{0j}$  to be independent of  $y$ . The leading-order solution is then written as

$$u_{0j} = \frac{1}{\gamma_j} , \quad v_{0j} = \gamma_j w , \quad (2.5)$$

where  $\gamma_j = \gamma_j(\sigma)$ , referred to as the amplitude of the  $j^{\text{th}}$  spike, is to be found. Here  $w(y)$  satisfies

$$w'' - w + w^2 = 0 , \quad -\infty < y < \infty ; \quad w(\pm\infty) = 0 , \quad w(0) > 0 . \quad (2.6)$$

The unique homoclinic of (2.6) is  $w = \frac{3}{2} \text{sech}^2(y/2)$ . Therefore, from (2.4), we get

$$\mathcal{L}v_{1j} \equiv v''_{1j} - v_{1j} + 2wv_{1j} = -\gamma_j^2 w^2 u_{1j} - x'_j \gamma_j w' , \quad (2.7a)$$

$$Du''_{1j} = \gamma_j w^2 . \quad (2.7b)$$

Since  $\mathcal{L}w' = 0$ , the solvability condition for (2.7a) yields that

$$x'_j \int_{-\infty}^{\infty} (w')^2 dy = -\frac{\gamma_j}{3} \int_{-\infty}^{\infty} u_{1j} \frac{d}{dy} (w^3) dy . \quad (2.8)$$

Integrating the right-hand side of (2.8) by parts twice, and using the facts that  $w$  and  $u''_{1j}$  are even functions of  $y$ , we readily derive that

$$x'_j \int_{-\infty}^{\infty} (w')^2 dy = \frac{\gamma_j}{6} [u'_{1j}(+\infty) + u'_{1j}(-\infty)] \int_{-\infty}^{\infty} w^3 dy . \quad (2.9)$$

Upon using the explicit form of  $w$  to evaluate the integrals in (2.9) we get

$$x'_j = \gamma_j [u'_{1j}(+\infty) + u'_{1j}(-\infty)] , \quad j = 1, \dots, k . \quad (2.10)$$

Now consider the outer region defined away from  $x_j$  for  $j = 1, \dots, k$ . Since the term  $\varepsilon^{-1} uv^2$  in (1.1b) is localized near each  $x = x_j$ , its effect on the outer solution for  $u$  can be calculated in the sense of distributions. From (2.2a), and  $\int_{-\infty}^{\infty} w^2 dy = 6$ , we obtain that

$$\varepsilon^{-1} uv^2 \rightarrow \sum_{j=1}^k \gamma_j \left( \int_{-\infty}^{\infty} w^2 dy \right) \delta(x - x_j) = \sum_{j=1}^k 6\gamma_j \delta(x - x_j) . \quad (2.11)$$

This leads to the outer problem for  $u(x, \sigma)$  given by

$$\tau \varepsilon^2 \mathcal{A}^2 u_\sigma = D u_{xx} + (1 - u) - \sum_{j=1}^k 6\gamma_j \delta(x - x_j), \quad |x| \leq 1,$$

with  $u_x = 0$  at  $x = \pm 1$ . The matching condition between the inner and outer solutions for  $u$  yields

$$u(x_j(\sigma), \sigma) = \frac{1}{\gamma_j \mathcal{A}^2} \ll 1, \quad u_x(x_j^\pm(\sigma), \sigma) = u'_{1j}(\pm\infty). \quad (2.12)$$

We summarize our asymptotic construction as follows:

**Principal Result 2.1:** *Assume that  $\tau \varepsilon^3 \mathcal{A}^2 \ll 1$ . Then, in the intermediate regime  $O(1) \ll \mathcal{A} \ll O(\varepsilon^{-1/2})$ , the GS model (1.1) can be reduced to the coupled ODE-PDE Stefan problem*

$$\tau \varepsilon^2 \mathcal{A}^2 u_\sigma = D u_{xx} + (1 - u) - \sum_{j=1}^k 6\gamma_j \delta(x - x_j), \quad |x| \leq 1, \quad (2.13a)$$

$$\frac{dx_j}{d\sigma} = \gamma_j \left[ u_x(x_j^+, \sigma) + u_x(x_j^-, \sigma) \right], \quad j = 1, \dots, k, \quad (2.13b)$$

$$u(x_j(\sigma), \sigma) = \frac{1}{\gamma_j \mathcal{A}^2}, \quad j = 1, \dots, k, \quad (2.13c)$$

with  $u_x(\pm 1, \sigma) = 0$ . Here  $\sigma = \varepsilon^2 \mathcal{A}^2 t$  is the slow timescale, and  $x_j(\sigma)$  is the center of  $j^{\text{th}}$  spike.

We observe that (2.13a) is a heat equation with singular Dirac source terms, and that (2.13b) become explicit ODE's only when we can determine  $u_x(x_j^\pm, \sigma)$  analytically. Finally, the constraints in (2.13c) implicitly determine the spike amplitudes  $\gamma_j(\sigma)$ , for  $j = 1, \dots, k$ .

## 2.1 Multi-Spike Quasi-Equilibria: The Quasi-Steady Limit $\tau \varepsilon^2 \mathcal{A}^2 \ll 1$

We suppose that  $\tau \ll \varepsilon^{-2} \mathcal{A}^{-2}$  so that  $u$  in (2.13a) is quasi-steady. With this assumption, we readily calculate from (2.13a), together with  $u_x = 0$  at  $x = \pm 1$ , that

$$u = \begin{cases} 1 - g_1 \frac{\cosh(\theta(x+1))}{\cosh(\theta(x_1+1))}, & -1 \leq x < x_1 \\ 1 - g_j \frac{\sinh(\theta(x_{j+1}-x))}{\sinh(\theta(x_{j+1}-x_j))} - g_{j+1} \frac{\sinh(\theta(x-x_j))}{\sinh(\theta(x_{j+1}-x_j))}, & x_j \leq x \leq x_{j+1}, \quad j = 1, \dots, k-1, \\ 1 - g_k \frac{\cosh(\theta(1-x))}{\cosh(\theta(1-x_k))}, & x_k < x \leq 1. \end{cases} \quad (2.14)$$

Here  $\theta \equiv D^{-1/2}$  and  $u = 1 - g_j$  at  $x = x_j$ . From this solution we calculate  $u_x$  as  $x \rightarrow x_j^\pm$ , and we impose the required jump conditions  $[Du_x]_j = 6\gamma_j$  for  $j = 1, \dots, k$  as seen from (2.13a). Here  $[\zeta]_j \equiv \zeta(x_j^+) - \zeta(x_j^-)$ . This leads to the following matrix problem

$$\mathcal{B} \mathbf{g} = \frac{6}{\sqrt{D}} \Gamma \mathbf{e}, \quad (2.15)$$

where the matrices  $\mathcal{B}$  and  $\Gamma$  and the vectors  $\mathbf{g}$  and  $\mathbf{e}$  are defined by

$$\mathcal{B} \equiv \begin{pmatrix} c_1 & d_1 & 0 & \cdots & 0 \\ d_1 & c_2 & d_2 & \cdots & 0 \\ \vdots & \ddots & \ddots & \ddots & \vdots \\ 0 & \cdots & d_{k-2} & c_{k-1} & d_{k-1} \\ 0 & \cdots & 0 & d_{k-1} & c_k \end{pmatrix}, \quad \Gamma \equiv \begin{pmatrix} \gamma_1 & \cdots & 0 \\ \vdots & \ddots & \vdots \\ 0 & \cdots & \gamma_k \end{pmatrix}, \quad \mathbf{g} \equiv \begin{pmatrix} g_1 \\ \vdots \\ g_k \end{pmatrix}, \quad \mathbf{e} \equiv \begin{pmatrix} 1 \\ \vdots \\ 1 \end{pmatrix}. \quad (2.16)$$

The matrix entries of  $\mathcal{B}$  are given explicitly by

$$\begin{aligned} c_1 &= \coth(\theta(x_2 - x_1)) + \tanh(\theta(1 + x_1)), & c_k &= \coth(\theta(x_k - x_{k-1})) + \tanh(\theta(1 - x_k)), \\ c_j &= \coth(\theta(x_{j+1} - x_j)) + \coth(\theta(x_j - x_{j-1})), & \text{for } j &= 2, \dots, k-1, \\ d_j &= -\operatorname{csch}(\theta(x_{j+1} - x_j)), & \text{for } j &= 1, \dots, k-1. \end{aligned} \quad (2.17)$$

Next, we write the constraint (2.13c) in matrix form as

$$\mathbf{g} = \mathbf{e} - \frac{1}{\mathcal{A}^2} \Gamma^{-1} \mathbf{e}. \quad (2.18)$$

Upon combining (2.18) and (2.15), we obtain that  $\gamma = (\gamma_1, \dots, \gamma_k)^t$  is given by

$$\gamma = \frac{\sqrt{D}}{6} \left( \mathcal{B} \mathbf{e} - \frac{1}{\mathcal{A}^2} \mathcal{B} \Gamma^{-1} \mathbf{e} \right). \quad (2.19)$$

Since  $\Gamma^{-1}$  depends on  $\gamma$ , (2.19) is a nonlinear algebraic system for the spike amplitudes  $\gamma_j$  for  $j = 1, \dots, k$ . However, since  $\mathcal{A} \gg 1$ , we can solve (2.19) asymptotically to obtain the explicit two-term expansion

$$\gamma = \frac{\sqrt{D}}{6} \mathcal{B} \left( I - \frac{6}{\mathcal{A}^2 \sqrt{D}} \Gamma_0^{-1} \right) \mathbf{e} + O(\mathcal{A}^{-4}), \quad (2.20)$$

where  $I$  is the identity matrix. Here  $\Gamma_0^{-1}$  is the inverse of the diagonal matrix  $\Gamma_0$  defined by

$$\Gamma_0 \equiv \begin{pmatrix} (\mathcal{B} \mathbf{e})_1 & \cdots & 0 \\ \vdots & \ddots & \vdots \\ 0 & \cdots & (\mathcal{B} \mathbf{e})_k \end{pmatrix}, \quad (2.21)$$

where  $(\mathcal{B} \mathbf{e})_j$  denotes the  $j^{\text{th}}$  component of the vector  $\mathcal{B} \mathbf{e}$ . Upon using the identity  $\coth \mu - \operatorname{csch} \mu = \tanh(\mu/2)$ , we can write (2.20) component-wise as

$$\gamma_j = \frac{\sqrt{D}}{6} (\mathcal{B} \mathbf{e})_j \left( 1 - \frac{6}{\mathcal{A}^2 \sqrt{D}} r_j \right) + O(\mathcal{A}^{-4}), \quad r_j \equiv \frac{(\mathcal{B} \Gamma_0^{-1} \mathbf{e})_j}{(\mathcal{B} \mathbf{e})_j}, \quad (2.22a)$$

where

$$(\mathcal{B} \mathbf{e})_j = \begin{pmatrix} \tanh\left(\frac{\theta}{2}(x_2 - x_1)\right) + \tanh(\theta(1 + x_1)) \\ \vdots \\ \tanh\left(\frac{\theta}{2}(x_j - x_{j-1})\right) + \tanh\left(\frac{\theta}{2}(x_{j+1} - x_j)\right) \\ \vdots \\ \tanh\left(\frac{\theta}{2}(x_k - x_{k-1})\right) + \tanh(\theta(1 - x_k)) \end{pmatrix}. \quad (2.22b)$$

With this approximation, and by noting that  $\Gamma^{-1} \sim \frac{6}{\sqrt{D}} \Gamma_0^{-1}$  for  $\mathcal{A} \gg 1$ , (2.18) reduces asymptotically to

$$\mathbf{g} = \mathbf{e} - \frac{6}{\mathcal{A}^2 \sqrt{D}} \Gamma_0^{-1} \mathbf{e} + O(\mathcal{A}^{-4}). \quad (2.23)$$

This asymptotically determines the unknown constants  $g_j$  for  $j = 1, \dots, k$  in (2.14) with an error  $O(\mathcal{A}^{-4})$ .

Next, we derive an explicit form for the ODE's in (2.13b). By calculating  $u_x(x_j^\pm)$  from (2.14), we readily derive that  $\mathbf{x}' = (x'_1, \dots, x'_k)^t$  satisfies

$$\mathbf{x}' = -\frac{1}{\sqrt{D}}\Gamma\mathcal{Q}\mathbf{g}, \quad (2.24)$$

where  $\mathcal{Q}$  is the tridiagonal matrix defined by

$$\mathcal{Q} \equiv \begin{pmatrix} e_1 & f_1 & 0 & \cdots & 0 \\ -f_1 & e_2 & f_2 & \cdots & 0 \\ \vdots & \ddots & \ddots & \ddots & \vdots \\ 0 & \cdots & -f_{k-2} & e_{k-1} & f_{k-1} \\ 0 & \cdots & 0 & -f_{k-1} & e_k \end{pmatrix}, \quad (2.25a)$$

with matrix entries

$$\begin{aligned} e_1 &= -\coth(\theta(x_2 - x_1)) + \tanh(\theta(1 + x_1)), & e_k &= \coth(\theta(x_k - x_{k-1})) - \tanh(\theta(1 - x_k)), \\ e_j &= -\coth(\theta(x_{j+1} - x_j)) + \coth(\theta(x_j - x_{j-1})), & \text{for } j &= 2, \dots, k-1, \\ f_j &= \operatorname{csch}(\theta(x_{j+1} - x_j)), & \text{for } j &= 1, \dots, k-1. \end{aligned} \quad (2.25b)$$

Finally, by combining (2.24) and (2.18), we obtain the following asymptotic result for the dynamics of  $k$ -spike quasi-equilibria:

**Principal Result 2.2:** *Assume that  $\tau\varepsilon^2\mathcal{A}^2 \ll 1$  and  $O(1) \ll \mathcal{A} \ll O(\varepsilon^{-1/2})$ . Then, the quasi-equilibrium solution for  $v(x, \sigma)$  is*

$$v(x, \sigma) \sim \sum_{j=1}^k \gamma_j w[\varepsilon^{-1}(x - x_j(\sigma))], \quad (2.26)$$

where  $w(y) = \frac{3}{2}\operatorname{sech}^2(y/2)$ . The corresponding outer approximation for  $u$  is given in (2.14) where the coefficients  $g_j$  in (2.14) for  $j = 1, \dots, k$  are given asymptotically in (2.23). For  $\mathcal{A} \gg 1$ , the spike amplitudes  $\gamma_j(\sigma)$  are given asymptotically in terms of the instantaneous spike locations  $x_j$  by (2.22a). Finally, the vector of spike locations satisfy the ODE system

$$\frac{d\mathbf{x}}{d\sigma} \sim -\frac{1}{\sqrt{D}}\Gamma\mathcal{Q}\left(I - \frac{6}{\mathcal{A}^2\sqrt{D}}\Gamma_0^{-1}\right)\mathbf{e}, \quad (2.27)$$

with  $\sigma = \varepsilon^2\mathcal{A}^2t$ . Here  $\Gamma_0$  is defined in (2.21) and  $\Gamma$  is defined in (2.16).

The equilibrium positions of the spikes satisfy  $\Gamma\mathcal{Q}\mathbf{g} = 0$ . In equilibrium,  $\gamma_j$  is a constant independent of  $j$ , and hence  $\mathbf{g} = c\mathbf{e}$  where  $c$  is some constant. Consequently, the equilibrium spike locations satisfy  $\mathcal{Q}\mathbf{e} = \mathbf{0}$ . By using (2.25), this leads to  $x_j = -1 + (2j - 1)/k$  for  $j = 1, \dots, k$ .

The leading-order approximation for the ODE's in (2.27) is obtained by using  $\Gamma \sim \frac{\sqrt{D}}{6}\Gamma_0 + O(\mathcal{A}^{-2})$ ,



and  $\mathbf{g} \sim \mathbf{e} + O(\mathcal{A}^{-2})$ . With this approximation, which neglects the  $O(\mathcal{A}^2)$  terms, (2.27) reduces to

$$\begin{aligned} x'_1 &\sim -\frac{1}{6} \left( \tanh^2 [\theta(1+x_1)] - \tanh^2 \left[ \frac{\theta}{2}(x_2-x_1) \right] \right), \\ x'_j &\sim -\frac{1}{6} \left( \tanh^2 \left[ \frac{\theta}{2}(x_j-x_{j-1}) \right] - \tanh^2 \left[ \frac{\theta}{2}(x_{j+1}-x_j) \right] \right), \quad j=1, \dots, k-1, \\ x'_k &\sim -\frac{1}{6} \left( \tanh^2 \left[ \frac{\theta}{2}(x_k-x_{k-1}) \right] - \tanh^2 [\theta(1-x_k)] \right). \end{aligned} \quad (2.28)$$

### 3 Oscillatory Profile Instabilities of $k$ -Spike Quasi-Equilibria

We now analyze the stability of the  $k$ -spike quasi-equilibrium solution of §2.1 to instabilities occurring on a fast  $O(1)$  time-scale. Since the spike locations drift slowly with speed  $O(\varepsilon^2 \mathcal{A}^2)$  (cf. (2.27)), in our stability analysis we make the asymptotic approximation that the spikes are at some fixed locations  $x_1, \dots, x_k$ . This asymptotic separation of time-scales with “frozen” spike locations allows for the derivation of a nonlocal eigenvalue problem (NLEP) governing fast instabilities.

Let  $u_e$  and  $v_e$  be the quasi-equilibrium solution constructed in §2.1. We substitute  $u(x, t) = u_e + e^{\lambda t} \eta(x)$  and  $v(x, t) = v_e + e^{\lambda t} \phi(x)$  into (1.1), and then linearize to obtain

$$\varepsilon^2 \phi_{xx} - \phi + 2\mathcal{A}u_e v_e \phi + \mathcal{A}v_e^2 \eta = \lambda \phi, \quad |x| \leq 1; \quad \phi_x(\pm 1) = 0, \quad (3.1a)$$

$$D\eta_{xx} - (1 + \tau\lambda)\eta - \varepsilon^{-1}v_e^2 \eta = 2\varepsilon^{-1}u_e v_e \phi, \quad |x| \leq 1; \quad \eta_x(\pm 1) = 0. \quad (3.1b)$$

We then look for a localized eigenfunction for  $\phi$  in the form

$$\phi(x) = \sum_{j=1}^k \phi_j [\varepsilon^{-1}(x - x_j)], \quad (3.2)$$

with  $\phi_j \rightarrow 0$  as  $|y| \rightarrow \infty$ . From (3.1a), and upon using  $v_e \sim \mathcal{A}\gamma_j w$  and  $u_e \sim 1/(\gamma_j \mathcal{A}^2)$  near  $x = x_j$ , we obtain on  $-\infty < y < \infty$  that  $\phi_j(y)$  satisfies

$$\phi_j'' - \phi_j + 2w\phi_j + \mathcal{A}^3 \gamma_j^2 w^2 \eta(x_j) = \lambda \phi_j. \quad (3.3)$$

Next, we consider (3.1b). Since  $\phi_j$  is localized near each spike, the spatially inhomogeneous coefficients in (3.1b) can be approximated by Dirac masses. In this way, and by using  $v_e \sim \mathcal{A}\gamma_j w$ ,  $u_e \sim 1/(\gamma_j \mathcal{A}^2)$ , and  $\int_{-\infty}^{\infty} w^2 dy = 6$ , we obtain for  $x$  near  $x_j$  that

$$2\varepsilon^{-1}u_e v_e \phi \sim \frac{2}{\mathcal{A}} \left( \int_{-\infty}^{\infty} w\phi_j dy \right) \delta(x - x_j), \quad \varepsilon^{-1}v_e^2 \sim 6\mathcal{A}^2 \gamma_j^2 \delta(x - x_j). \quad (3.4)$$

Therefore, the outer problem for  $\eta$  in (3.1b) becomes

$$D\eta_{xx} - \left[ 1 + \tau\lambda + 6\mathcal{A}^2 \sum_{j=1}^k \gamma_j^2 \delta(x - x_j) \right] \eta = \sum_{j=1}^k \frac{2}{\mathcal{A}} \left( \int_{-\infty}^{+\infty} w\phi_j dy \right) \delta(x - x_j), \quad (3.5)$$

with  $\eta_x = 0$  at  $x = \pm 1$ . Defining  $[\xi]_j$  by  $[\xi]_j \equiv \xi(x_{j+}) - \xi(x_{j-})$ , we obtain the equivalent problem

$$D\eta_{xx} - (1 + \tau\lambda)\eta = 0, \quad |x| \leq 1; \quad \eta_x(\pm 1) = 0, \quad (3.6a)$$

$$[\eta]_j = 0, \quad [D\eta_x]_j = -6\omega_j + 6\mathcal{A}^2\gamma_j^2\eta(x_j), \quad j = 1, \dots, k; \quad \omega_j \equiv -\frac{2}{\mathcal{A}} \left( \frac{\int_{-\infty}^{\infty} w\phi_j dy}{\int_{-\infty}^{\infty} w^2 dy} \right). \quad (3.6b)$$

Next, we calculate  $\eta_j \equiv \eta(x_j)$  from (3.6), which is needed in (3.3). To do so, we solve (3.6a) on each subinterval and then use the jump conditions in (3.6b). This leads to the matrix problem

$$\mathcal{E}_\lambda \boldsymbol{\eta} = \frac{6}{[D(1 + \tau\lambda)]^{1/2}} \boldsymbol{\omega}, \quad (3.7)$$

where the vectors  $\boldsymbol{\omega}$  and  $\boldsymbol{\eta}$  are defined by  $\boldsymbol{\omega}^t = (\omega_1, \dots, \omega_k)$  and  $\boldsymbol{\eta}^t = (\eta_1, \dots, \eta_k)$ , and where  $t$  denotes transpose. The matrix  $\mathcal{E}_\lambda$  in (3.7) is defined in terms of a tridiagonal matrix  $\mathcal{B}_\lambda$  by

$$\mathcal{E}_\lambda \equiv \mathcal{B}_\lambda + \frac{6\mathcal{A}^2}{\sqrt{D(1 + \tau\lambda)}} \Gamma^2, \quad \mathcal{B}_\lambda \equiv \begin{pmatrix} c_{1,\lambda} & d_{1,\lambda} & 0 & \cdots & 0 \\ d_{1,\lambda} & \ddots & \ddots & \ddots & \vdots \\ 0 & \ddots & \ddots & \ddots & 0 \\ \vdots & \ddots & \ddots & \ddots & d_{k-1,\lambda} \\ 0 & \cdots & 0 & d_{k-1,\lambda} & c_{k,\lambda} \end{pmatrix}. \quad (3.8)$$

Here  $\Gamma$  is the diagonal matrix of spike amplitudes defined in (2.16). The matrix entries of  $\mathcal{B}_\lambda$  are

$$\begin{aligned} c_{1,\lambda} &= \coth(\theta_\lambda(x_2 - x_1)) + \tanh(\theta_\lambda(1 + x_1)), & c_{k,\lambda} &= \coth(\theta_\lambda(x_k - x_{k-1})) + \tanh(\theta_\lambda(1 - x_k)), \\ c_{j,\lambda} &= \coth(\theta_\lambda(x_{j+1} - x_j)) + \coth(\theta_\lambda(x_j - x_{j-1})), & j &= 2, \dots, k-1, \\ d_{j,\lambda} &= -\operatorname{csch}(\theta_\lambda(x_{j+1} - x_j)), & j &= 1, \dots, k-1. \end{aligned} \quad (3.9)$$

In (3.9),  $\theta_\lambda$  is the principal branch of the square root for  $\theta_\lambda \equiv \theta_0\sqrt{1 + \tau\lambda}$ , with  $\theta_0 \equiv D^{-1/2}$ . Notice that when  $\lambda = 0$ ,  $\mathcal{B}_\lambda = \mathcal{B}$ , where  $\mathcal{B}$  was defined in (2.16).

Next, we invert (3.7) to obtain

$$\boldsymbol{\eta} = \frac{1}{[D(1 + \tau\lambda)]^{1/2}} \mathcal{E}_\lambda^{-1} \boldsymbol{\omega} = -\frac{12}{\mathcal{A}\sqrt{D(1 + \tau\lambda)}} \left( \frac{\int_{-\infty}^{\infty} w(\mathcal{E}_\lambda^{-1}\boldsymbol{\phi}) dy}{\int_{-\infty}^{\infty} w^2 dy} \right), \quad (3.10)$$

where  $\boldsymbol{\phi}^t = (\phi_1, \dots, \phi_k)$ . Substituting (3.10) into (3.3), we obtain the following nonlocal eigenvalue problem (NLEP) in terms of a new matrix  $\mathcal{C}_\lambda$ :

$$\boldsymbol{\phi}'' - \boldsymbol{\phi} + 2w\boldsymbol{\phi} - w^2 \left( \frac{\int_{-\infty}^{\infty} w(\mathcal{C}_\lambda\boldsymbol{\phi}) dy}{\int_{-\infty}^{\infty} w^2 dy} \right) = \lambda\boldsymbol{\phi}; \quad \mathcal{C}_\lambda \equiv \frac{12\mathcal{A}^2}{\sqrt{D(1 + \tau\lambda)}} \Gamma^2 \mathcal{E}_\lambda^{-1}. \quad (3.11)$$

Since  $\Gamma$  is a positive definite diagonal matrix and  $\mathcal{E}_\lambda$  is symmetric, we can decompose  $\mathcal{C}_\lambda$  into its eigenvalues and eigenvectors as

$$\mathcal{C}_\lambda = \mathcal{S}\mathcal{X}\mathcal{S}^{-1}, \quad (3.12)$$

where  $\mathcal{X}$  is the diagonal matrix of eigenvalues  $\chi_j$  of  $\mathcal{C}_\lambda$  and  $\mathcal{S}$  is the matrix of its eigenvectors  $\mathbf{s}_j$ . We then set  $\boldsymbol{\psi} = \mathcal{S}^{-1}\boldsymbol{\phi}$  to diagonalize (3.11), and we rewrite  $\mathcal{C}_\lambda$  in terms of  $\mathcal{B}_\lambda$  by using (3.8). This leads to the following stability criterion for fast instabilities:

**Principal Result 3.1:** *The  $k$ -spike quasi-equilibrium solution of §2.1 with fixed spike locations is stable on a fast  $O(1)$  time-scale if the following  $k$  NLEP problems on  $-\infty < y < \infty$ , given by*

$$\psi'' - \psi + 2w\psi - \chi_j(\tau\lambda)w^2 \left( \frac{\int_{-\infty}^{\infty} w\psi dy}{\int_{-\infty}^{\infty} w^2 dy} \right) = \lambda\psi; \quad \psi \rightarrow 0 \quad \text{as } |y| \rightarrow \infty, \quad (3.13)$$

only have eigenvalues that satisfy  $\text{Re}\lambda < 0$ . Here  $\chi_j(\tau\lambda)$  for  $j = 1, \dots, k$ , are the eigenvalues of the matrix  $\mathcal{C}_\lambda$  defined by

$$\mathcal{C}_\lambda = 2 \left[ I + \frac{\sqrt{D(1+\tau\lambda)}}{6\mathcal{A}^2} \mathcal{B}_\lambda \Gamma^{-2} \right]^{-1}. \quad (3.14)$$

We now analyze (3.13). Let  $\tau = O(1)$  and assume that the inter-spike distances  $d_j = x_{j+1} - x_j$  for  $j = 0, \dots, k$  are  $O(1)$ . Here, for  $j = 0$  and  $j = k$  we define  $d_0 = x_1 + 1$  and  $d_k = 1 - x_k$ , respectively. Then, for  $\mathcal{A} \gg 1$ , (3.14) yields  $\mathcal{C}_\lambda \sim 2I$  so that  $\chi_j \sim 2$  for  $j = 1, \dots, k$ . Since  $\chi_j$  is a constant with  $\chi_j > 1$  in this limit, the result of Theorem 1.4 of [35] proves that  $\text{Re}(\lambda) < 0$ . This guarantees stability for  $\mathcal{A} \gg 1$  when  $\tau = O(1)$  and  $d_j = x_{j+1} - x_j = O(1)$ .

Next, we consider the limit  $\mathcal{A} \gg 1$ ,  $\tau = O(1)$ , but we will allow for the inter-spike distances  $d_j = x_{j+1} - x_j$  to be small but with  $d_j \gg O(\varepsilon)$ . Recall that the analysis of §2 and §3 leading to Principal Result 3.1 required that  $d_j \gg O(\varepsilon)$ . We will show that for the scaling regime  $d_j = O(\mathcal{A}^{-2/3}) \gg O(\varepsilon)$  of closely spaced spikes, and with  $O(1) \ll \mathcal{A} \ll O(\varepsilon^{-1/2})$ , the NLEP problem (3.13) can have an unstable eigenvalue for any  $\tau > 0$ . For simplicity we will only consider a closely spaced equilibrium configuration with  $d_j = L \ll 1$  for  $j = 1, \dots, k-1$ , and  $d_0 = d_k = L/2$ . In this limit it is readily shown from (3.9) that

$$\mathcal{B}_\lambda \sim \frac{1}{\theta_\lambda L} \mathcal{B}_0, \quad \mathcal{B}_0 \equiv \begin{pmatrix} 1 & -1 & 0 & \dots & 0 \\ -1 & 2 & -1 & \dots & 0 \\ \vdots & \ddots & \ddots & \ddots & \vdots \\ 0 & \dots & -1 & 2 & -1 \\ 0 & \dots & 0 & -1 & 1 \end{pmatrix}. \quad (3.15)$$

Moreover, for  $\mathcal{A} \gg 1$  and with spikes of a uniform spacing  $L \ll 1$ , we obtain from (2.22) that the spikes have a common amplitude given by

$$\gamma_j \sim \frac{\sqrt{D}}{6} (\mathcal{B}e)_j = \frac{\sqrt{D}}{3} \tanh\left(\frac{\theta_0 L}{2}\right) \sim \frac{L}{6}. \quad (3.16)$$

Substituting (3.15) and (3.16) into (3.14), we obtain that the eigenvalues  $\chi_j$  of  $\mathcal{C}_\lambda$  are given by

$$\chi_j \sim 2 \left[ 1 + \frac{\sqrt{D(1+\tau\lambda)}}{6\mathcal{A}^2} \left( \frac{36}{L^2} \right) \left( \frac{r_j}{\theta_\lambda L} \right) \right]^{-1} = 2 \left[ 1 + \frac{6Dr_j}{\mathcal{A}^2 L^3} \right]^{-1}, \quad (3.17)$$

where  $r_j$  for  $j = 1, \dots, k$  are the eigenvalues of the matrix  $\mathcal{B}_0$  defined in (3.15). Appendix E of [13] and Theorem 1.4 of [35] proves that when  $\chi_j$  is constant, then  $\text{Re}(\lambda) > 0$  if and only if  $\chi_j < 1$  for  $j = 1, \dots, k$ .

Therefore, the stability threshold is determined by  $\chi_m \equiv \min_{j=1,\dots,k}(\chi_j) = 1$ , which depends on the largest eigenvalue  $r_m \equiv \max_{j=1,\dots,k}(r_j)$  of  $\mathcal{B}_0$ . By calculating this largest eigenvalue, and by setting  $\chi_m = 1$ , we obtain that the  $k$ -spike equilibrium solution is unstable for any  $\tau > 0$  on the regime  $O(1) \ll \mathcal{A} \ll O(\varepsilon^{-1/2})$  when  $L < L_*$ , where

$$L_* \equiv \left( \frac{6Dr_m}{\mathcal{A}^2} \right)^{1/3}, \quad r_m \equiv 2[1 + \cos(\pi/k)]. \quad (3.18)$$

The result (3.18) shows that competition instabilities in the intermediate regime  $O(1) \ll \mathcal{A} \ll O(\varepsilon^{-1/2})$  can only occur if the spikes are sufficiently close with inter-spike separation  $O(\mathcal{A}^{-2/3})$ . If we did set  $\mathcal{A} = O(1)$  in (3.18), then  $L_* = O(1)$  is consistent with the scalings in [17] and [31] for competition instabilities of equilibrium and quasi-equilibrium spike patterns in the low feed-rate regime  $\mathcal{A} = O(1)$ .

Next, we obtain our main instability result that oscillatory instabilities of  $k$ -spike quasi-equilibria can occur when  $\tau = O(\mathcal{A}^4) \gg 1$  and with  $O(1)$  inter-spike separation distances. From the choice of the principal value of the square root, we obtain that  $\text{Re}(\theta_\lambda) = \theta_0 \text{Re}(\sqrt{1 + \tau\lambda}) \rightarrow +\infty$  on  $|\arg(\lambda)| < \pi$  as  $\tau \rightarrow \infty$ . Therefore, for  $\tau \gg 1$ , and for  $x_{j+1} - x_j = O(1)$ , we calculate from the matrix entries of  $\mathcal{B}_\lambda$  in (3.9) that  $\mathcal{B}_\lambda \rightarrow 2I$  in  $|\arg(\lambda)| < \pi$ . Therefore, with  $\tau = \tilde{\tau}\mathcal{A}^4$ , where  $\tilde{\tau} = O(1)$ , we get from (3.14) that

$$\mathcal{C}_\lambda \sim 2 \left[ I + \frac{\sqrt{D\tilde{\tau}\lambda}}{3} \Gamma^{-2} \right]^{-1}, \quad (3.19)$$

where  $\Gamma$  is the diagonal matrix of spike amplitudes  $\gamma_j$  for  $j = 1, \dots, k$ . This form suggests that we define  $\tau_H$  by  $\tilde{\tau} = 9D^{-1}\gamma_j^4\tau_H$ , so that  $\mathcal{C} \sim 2[1 + \sqrt{\tau_H\lambda}]^{-1}I$ . This limiting matrix has only one distinct eigenvalue, and so in the scaling regime  $\tau = O(\mathcal{A}^4)$ , the stability of  $k$ -spike quasi-equilibria is determined by the NLEP (3.13) with the single multiplier

$$\chi_\infty = \frac{2}{1 + \sqrt{\tau_H\lambda}}, \quad \text{when } \tau = \frac{9\mathcal{A}^4\tau_H\gamma_j^4}{D} \gg 1. \quad (3.20)$$

This limiting NLEP problem was derived for equilibrium spike solutions in [4], [5], [22], and [17] in the intermediate regime. From the rigorous analysis of [5] and [17], it follows that this NLEP undergoes a Hopf bifurcation at some  $\tau_H = \tau_{H0}$ . From numerical computations it is known that  $\tau_{H0} \approx 1.748$ , and that  $\text{Re}(\lambda) < 0$  only when  $\tau_H < \tau_{H0}$  (cf. [4], [17]). Although this limiting NLEP problem has a continuous spectrum on the non-negative real axis  $\Re\lambda \leq 0$ , there are no edge bifurcations arising from the end-point  $\lambda = 0$  (cf. [5], [17]).

With the scaling law for  $\tau$  in (3.20), we obtain  $k$  distinct values of  $\tau$  where complex conjugate eigenvalues appear on the imaginary axis. The minimum of these values determines the instability threshold for  $\tau$ . Finally, by using (2.22) to calculate the spike amplitudes asymptotically for  $\mathcal{A} \gg 1$ , we obtain the following main instability result:

**Principal Result 3.2:** *Let  $\tau = O(\mathcal{A}^4)$  with  $x_{j+1} - x_j = O(1)$  and  $O(1) \ll \mathcal{A} \ll O(\varepsilon^{-1/2})$ . Then, the frozen  $k$ -spike quasi-equilibrium solution of §2.1 develops an oscillatory instability due to a Hopf bifurcation when  $\tau$  increases past  $\tau_h$ , where*

$$\tau_h = \min_{j=1,\dots,k}(\tau_{hj}), \quad \tau_{hj} \sim \frac{D\mathcal{A}^4}{144} \tau_{H0} (\mathbf{Be})_j^4 \left( 1 - \frac{6}{\mathcal{A}^2\sqrt{D}} r_j \right)^4, \quad j = 1, \dots, k. \quad (3.21)$$

Here  $\tau_{H0} \approx 1.748$ , while  $(\mathcal{B}\mathbf{e})_j$  and  $r_j$  are defined in terms of the spike locations by (2.22).

For an equilibrium  $k$ -spike pattern where  $x_j = -1 + (2j - 1)/k$  for  $j = 1, \dots, k$ , we calculate from (2.22b) that  $(\mathcal{B}\mathbf{e})_j = 2 \tanh(\theta_0/k)$  and  $r_j = [2 \tanh(\theta_0/k)]^{-1}$  for  $j = 1, \dots, k$ . This leads to the equilibrium stability threshold

$$\tau_h \sim \frac{D\mathcal{A}^4}{9} \tau_{H0} \tanh^4\left(\frac{\theta_0}{k}\right) \left(1 - \frac{3}{\mathcal{A}^2 \sqrt{D} \tanh(\theta_0/k)}\right)^4, \quad (3.22)$$

which agrees asymptotically with that given in Proposition 4.3 of [17].

An important remark concerns the range of validity of Principal Result 3.2 with respect to  $\tau$ . The derivation of (3.21) assumed that  $\tau \varepsilon^2 \mathcal{A}^2 \ll 1$ , while the scaling law for instabilities predicts that  $\tau = O(\mathcal{A}^4)$ . Therefore, we conclude that (3.21) only holds in the subregime  $O(1) \ll \mathcal{A} \ll O(\varepsilon^{-1/3})$  of the intermediate regime.

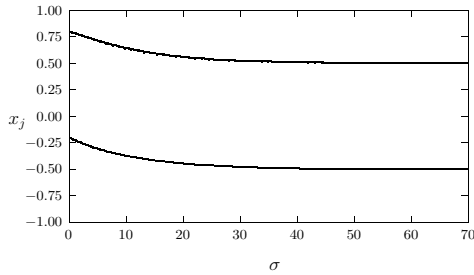
### 3.1 Numerical Experiments of Quasi-Equilibrium Spike Layer Motion

We now give two examples illustrating our results of §2 and §3 for slow spike dynamics.

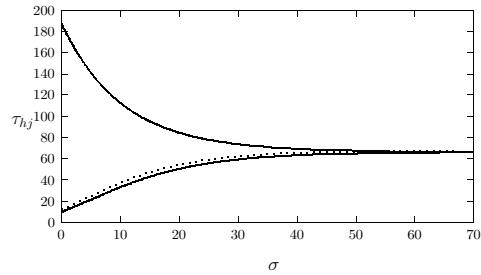
#### *Experiment 3.1: A two-spike evolution*

Consider a two-spike evolution with parameter values  $D = 1.0$ ,  $\mathcal{A} = 10.0$ ,  $\tau = 5.0$ , and  $\varepsilon = 0.005$ . The initial spike locations are  $x_1(0) = -0.20$  and  $x_2(0) = 0.80$ . In Fig 2(a) we plot the spike layer trajectories versus the slow time  $\sigma$ , computed numerically from (2.27), which shows the gradual approach to the equilibrium values at  $x_1 = -1/2$  and  $x_2 = 1/2$ . In Fig. 2(c) we plot the spike amplitudes versus  $\sigma$ . A plot of the quasi-equilibrium solution at several instants in time is shown in Fig. 2(d). In Fig. 2(b) we plot the two Hopf bifurcation values  $\tau_{hj}$ , for  $j = 1, 2$ , versus  $\sigma$  calculated from (3.21). In these figures the solid curves were obtained when computing for the spike amplitudes from the nonlinear algebraic system (2.19), while the dotted lines result from using the corresponding two-term approximation (2.20). An important observation from Fig. 2(b) is that the stability threshold  $\tau_h(\sigma)$ , defined by  $\tau_h(\sigma) \equiv \min_{j=1,2} [\tau_{hj}(\sigma)]$ , is an increasing function of  $\sigma$  with  $\tau_h(0) \approx 12.5$  and  $\tau_h(\infty) \approx 67.7$ . This monotone behavior of  $\tau_h(\sigma)$ , together with the initial value  $\tau_h(0) > \tau = 5.0$ , implies that there is no dynamic triggering of an oscillatory instability in the spike amplitudes before the equilibrium two-spike pattern is reached.

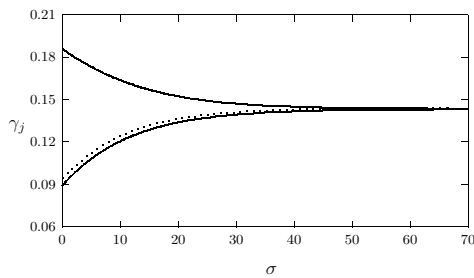
More generally, we have been unable to prove analytically from the DAE system (2.27) and (2.20) that the stability threshold  $\tau_h(\sigma) \equiv \min_{j=1,\dots,k} (\tau_{hj}(\sigma))$  of (3.21) must always be an increasing function of  $\sigma$ . However, we have performed many numerical experiments to examine this condition, and in each case we have found numerically that  $\tau_h(\sigma)$  is a monotonically increasing function of  $\sigma$ . This leads to the conjecture that there are no dynamically triggered oscillatory instabilities of multi-spike quasi-equilibria in the intermediate regime  $O(1) \ll \mathcal{A} \ll O(\varepsilon^{-1/2})$ . In other words,  $\tau < \tau_h(0)$  is a sufficient condition for stability of the quasi-equilibrium multi-spike pattern for all  $\sigma > 0$ . In contrast, for the simple case of symmetric two-spike quasi-equilibria in the low feed-rate regime  $\mathcal{A} = O(1)$ , dynamically triggered instabilities due to either Hopf bifurcations or from the creation of a real positive eigenvalue were established analytically in [31].



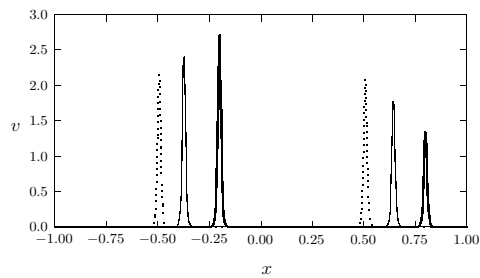
(a)  $x_j$  vs.  $\sigma$



(b)  $\tau_{hj}$  vs.  $\sigma$



(c)  $\gamma_j$  vs.  $\sigma$



(d)  $v$  vs.  $x$

Figure 2: *Experiment 3.1*: Slow evolution of a two-spike quasi-equilibrium solution for  $\varepsilon = 0.005$ ,  $\mathcal{A} = 10$ , and  $D = 1.0$ , with  $x_1(0) = -0.2$  and  $x_2(0) = 0.8$ . Top Left:  $x_j$  vs.  $\sigma$ . Top Right:  $\tau_{hj}$  vs.  $\sigma$ . Bottom Left:  $\gamma_j$  vs.  $\sigma$ . Bottom Right:  $v$  vs.  $x$  at  $\sigma = 0$  (heavy solid curve),  $\sigma = 10$  (solid curve), and  $\sigma = 50$  (dotted curve). Except for the plot at the bottom right, the solid lines result from a numerical solution of the spike amplitudes from (2.19), while the dotted lines are from the two-term approximation (2.20).

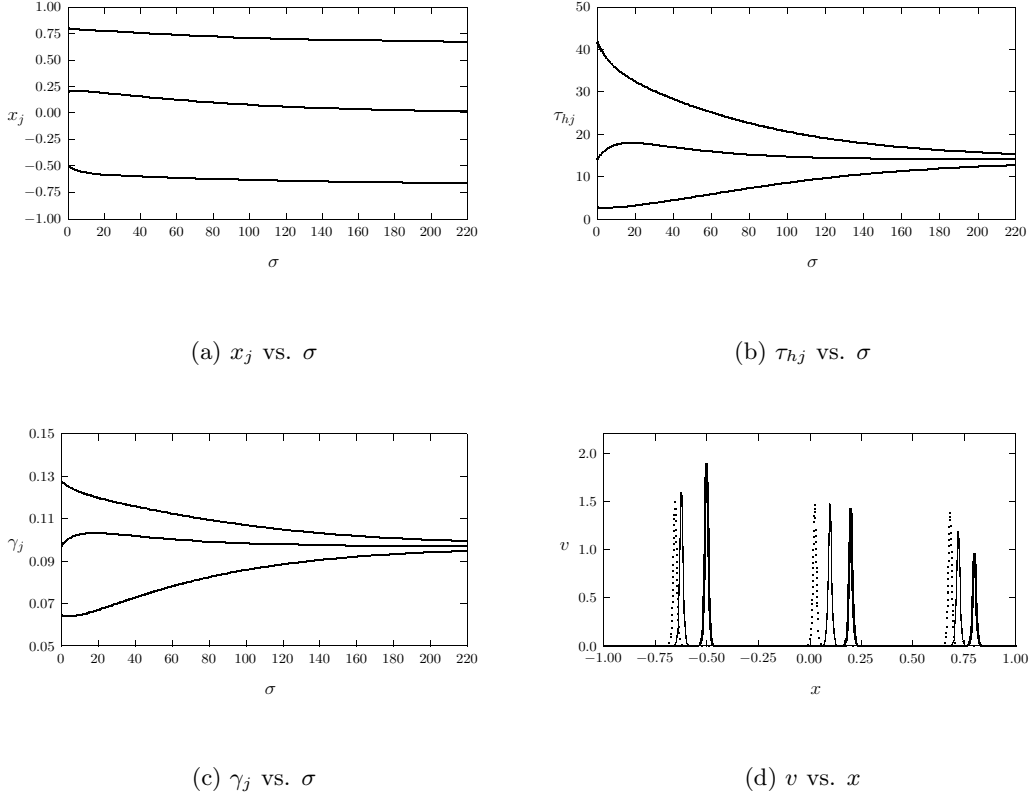


Figure 3: *Experiment 3.2*: Slow evolution of a three-spike quasi-equilibrium solution for  $\varepsilon = 0.005$ ,  $\mathcal{A} = 10$ , and  $D = 1.0$ , with  $x_1(0) = -0.5$ ,  $x_2(0) = 0.2$ , and  $x_3(0) = 0.80$ , obtained from the two-term asymptotic result (2.20) for the spike amplitudes. Top Left:  $x_j$  vs.  $\sigma$ . Top Right:  $\tau_{hj}$  vs.  $\sigma$ . Bottom Left:  $\gamma_j$  vs.  $\sigma$ . Bottom Right:  $v$  vs.  $x$  at  $\sigma = 0$  (heavy solid curve),  $\sigma = 80$  (solid curve), and  $\sigma = 200$ .

### *Experiment 3.2: A three-spike evolution*

Next, we consider a three-spike evolution with parameter values  $D = 1.0$ ,  $\mathcal{A} = 10.0$ ,  $\tau = 2.0$ , and  $\varepsilon = 0.005$ . The initial spike locations are  $x_1(0) = -0.50$ ,  $x_2(0) = 0.20$ , and  $x_3(0) = 0.80$ . In Fig 3(a) and Fig 3(c) we plot the the spike layer trajectories and spike amplitudes, respectively, computed from (2.27) and the two-term approximation (2.20). Snapshots of the quasi-equilibrium solution are shown in Fig. 3(d). In Fig. 3(b) we plot the three Hopf bifurcation values  $\tau_{hj}$ , for  $j = 1, \dots, 3$ , versus  $\sigma$  calculated from (3.21). From Fig. 2(b) we observe that the stability threshold  $\tau_h(\sigma) \equiv \min_{j=1,2,3} [\tau_{hj}(\sigma)]$ , is an increasing function of  $\sigma$  with  $\tau_h(0) \approx 2.6$  and  $\tau_h(\infty) \approx 14.0$ . This monotonicity of  $\tau_h(\sigma)$ , together with  $\tau_h(0) > \tau = 2.0$ , again precludes the existence of a dynamically triggered Hopf bifurcation in the spike amplitudes.

## 4 Oscillatory Drift Instabilities of $k$ -Spike Patterns

In this section we compute numerical solutions to the Stefan problem (2.13) when  $\tau\epsilon^2\mathcal{A}^2 = O(1)$  and  $O(\epsilon^{-1/3}) \ll \mathcal{A} \ll O(\epsilon^{-1/2})$ . For notational convenience, so as not to confuse spike locations with gridpoints of the discretization, we re-label the spike trajectories as  $\xi_j(\sigma)$ , for  $j = 1, \dots, k$ . Then, defining  $\tau_0 \equiv \epsilon^{-2}\mathcal{A}^{-2}\tau = O(1)$  to be the key bifurcation parameter, (2.13) becomes

$$\tau_0 u_\sigma = Du_{xx} + (1 - u) - \sum_{j=1}^k 6\gamma_j \delta(x - \xi_j), \quad |x| \leq 1; \quad u_x(\pm 1, \sigma) = 0, \quad (4.1a)$$

$$\xi_j' = \gamma_j \left[ u_x(\xi_j^+, \sigma) + u_x(\xi_j^-, \sigma) \right], \quad j = 1, \dots, k, \quad (4.1b)$$

$$u(\xi_j(\sigma), \sigma) = 1/(\gamma_j \mathcal{A}^2), \quad j = 1, \dots, k. \quad (4.1c)$$

By using a singular limit eigenvalue problem (SLEP) method, which is related to the method pioneered in [24], it was shown in [19] that a one-spike equilibrium solution will become unstable at some critical value of  $\tau_0$  to an oscillatory drift instability associated with a pure imaginary small eigenvalue  $\lambda \ll 1$  of the linearization. As  $\tau_0$  increases above this critical value a complex conjugate pair of eigenvalues crosses into the right half-plane  $\text{Re}(\lambda) > 0$ , leading to the initiation of a small-scale oscillatory motion of the spike location. This oscillatory drift instability is the dominant instability mechanism in the subregime  $O(\epsilon^{-1/3}) \ll \mathcal{A} \ll O(\epsilon^{-1/2})$  of the intermediate regime.

We first show that the condition for the stability of the equilibrium solution to the Stefan problem (4.1) is equivalent to that obtained in [19] using the SLEP method. For simplicity, we consider the one-spike case where  $k = 1$ . We let  $U \equiv U(x)$  and  $\gamma = \gamma_{1e}$  denote the equilibrium solution to (4.1) with  $\xi_1 = 0$ . Then,

$$DU_{xx} + (1 - U) = 0, \quad |x| < 1; \quad U_x(\pm 1) = 0; \quad [DU_x]_0 = 6\gamma_{1e}; \quad U(0) = \frac{1}{\gamma_e \mathcal{A}^2}. \quad (4.2)$$

Here we have defined  $[v]_0 \equiv v(0^+) - v(0^-)$ . We readily calculate that

$$U = 1 - B \frac{\cosh(\theta_0(1+x))}{\cosh \theta_0}, \quad -1 \leq x < 0; \quad U = 1 - B \frac{\cosh(\theta_0(1-x))}{\cosh \theta_0}, \quad 0 < x \leq 1, \quad (4.3a)$$

where  $\theta_0 \equiv D^{-1/2}$ , and

$$\gamma_{1e} = \frac{B\sqrt{D}}{3} \tanh \theta_0, \quad B = 1 - \frac{1}{\gamma_{1e} \mathcal{A}^2}. \quad (4.3b)$$

By solving the quadratic equation for  $\gamma_{1e}$  we get

$$\gamma_{1e} = \frac{\sqrt{D}}{6} \tanh \theta_0 \left[ 1 + \sqrt{1 - \frac{\mathcal{A}_{1e}^2}{\mathcal{A}^2}} \right], \quad \mathcal{A}_{1e} \equiv \sqrt{\frac{12\theta_0}{\tanh \theta_0}}. \quad (4.3c)$$

For  $\mathcal{A} \gg 1$ , we readily obtain that

$$\gamma_{1e} = \frac{\sqrt{D}}{3} \tanh \theta_0 - \frac{1}{\mathcal{A}^2} + O(\mathcal{A}^{-4}), \quad B = 1 - \frac{3}{\mathcal{A}^2 \sqrt{D} \tanh \theta_0} + O(\mathcal{A}^{-4}). \quad (4.3d)$$



For  $\delta \ll 1$ , we perturb the equilibrium solution as

$$u(x, \sigma) = U(x) + \delta e^{\lambda \sigma} \phi(x), \quad \gamma_{1e} = \gamma_e + \delta \beta e^{\lambda \sigma}, \quad \xi_1 = \delta e^{\lambda \sigma}. \quad (4.4)$$

We substitute (4.4) into (4.1a), and collect  $O(\delta)$  terms to get  $D\phi_{xx} - (1 + \tau_0\lambda)\phi = 0$  on  $|x| \leq 1$ . From the linearization of the ODE (4.1b), we obtain

$$\delta \lambda e^{\lambda \sigma} = \left( \gamma_{1e} + \delta \beta e^{\lambda \sigma} \right) \left( U_x(0^+) + U_x(0^-) + \delta e^{\lambda \sigma} [\phi_x(0^+) + \phi_x(0^-) + U_{xx}(0^+) + U_{xx}(0^-)] \right). \quad (4.5a)$$

In addition, the conditions  $[Du_x]_{\xi_1} = 6\gamma_1$  and  $u(\xi_1) = 1/(\gamma_1 \mathcal{A}^2)$  become

$$D \left( U_x(0^+) - U_x(0^-) + \delta e^{\lambda \sigma} [U_{xx}(0^+) - U_{xx}(0^-) + \phi_x(0^+) - \phi_x(0^-)] \right) = 6 \left( \gamma_{1e} + \delta \beta e^{\lambda \sigma} \right), \quad (4.5b)$$

$$U(0^\pm) + \delta e^{\lambda t} (U_x(0^\pm) + \phi(0^\pm)) = \frac{1}{\gamma_{1e} \mathcal{A}^2} - \frac{\delta \beta}{\gamma_{1e}^2 \mathcal{A}^2} e^{\lambda \sigma}. \quad (4.5c)$$

Since  $U_x(0^+) + U_x(0^-) = 0$ ,  $U_{xx}(0^+) = U_{xx}(0^-)$ , and  $U_x(0^\pm) = \pm 3\gamma_{1e}/D$ , we collect the  $O(\delta)$  terms in (4.5) to obtain the following problem for  $\phi$ :

$$D\phi_{xx} - (1 + \tau_0\lambda)\phi = 0, \quad |x| \leq 1; \quad \phi_x(\pm 1) = 0, \quad (4.6a)$$

$$[D\phi_x]_0 = 6\beta; \quad \phi(0^\pm) = \mp \frac{3\gamma_{1e}}{D} - \frac{\beta}{\gamma_{1e}^2 \mathcal{A}^2}, \quad (4.6b)$$

$$\lambda = 2\gamma_e \left( U_{xx}(0) + \frac{1}{2} [\phi_x(0^+) + \phi_x(0^-)] \right). \quad (4.6c)$$

The solution to (4.6a) satisfying the prescribed values for  $\phi(0^\pm)$  is

$$\phi = C_- \frac{\cosh(\theta_\lambda(x+1))}{\cosh \theta_\lambda}, \quad -1 \leq x < 0; \quad u = C_+ \frac{\cosh(\theta_\lambda(1-x))}{\cosh \theta_\lambda}, \quad 0 < x \leq 1, \quad (4.7a)$$

where  $\theta_\lambda \equiv \theta_0 \sqrt{1 + \tau_0 \lambda}$ , and

$$C_\pm = \mp \frac{3\gamma_{1e}}{D} - \frac{\beta}{\gamma_{1e}^2 \mathcal{A}^2}. \quad (4.8)$$

The jump condition  $[D\phi_x]_0 = 6\beta$ , then yields that  $\beta = 0$ . Then, we substitute values for  $\phi_x(0^\pm)$  and  $U_{xx}(0) = -D^{-1} (1 - 1/(\gamma_{1e} \mathcal{A}^2))$  into (4.6c) to obtain

$$\lambda = 2\gamma_{1e} \left[ \frac{3\gamma_{1e}}{D} \theta_\lambda \tanh \theta_\lambda - \frac{1}{D} \left( 1 - \frac{1}{\gamma_{1e} \mathcal{A}^2} \right) \right]. \quad (4.9)$$

Finally, by using (4.3c) for  $\gamma_{1e}$ , we readily derive that  $\lambda$  satisfies the transcendental equation

$$\lambda = \mu \left[ \sqrt{1 + \tau_0 \lambda} \tanh \theta_0 \tanh \theta_\lambda - 1 \right], \quad \mu \equiv \frac{\theta_0}{6} \tanh \theta_0 \left[ 1 + \sqrt{1 - \frac{\mathcal{A}_{1e}^2}{\mathcal{A}^2}} \right]^2. \quad (4.10)$$

Here  $\theta_\lambda \equiv \theta_0 \sqrt{1 + \tau_0 \lambda}$ ,  $\theta_0 \equiv D^{-1/2}$ , while  $\mathcal{A}_{1e}$  is defined in (4.3c). This expression is the same as that obtained in equation (5.5) of [19] using the SLEP method based on a linearization of (1.1) around a one-spike equilibrium solution.

We introduce  $\omega$ ,  $\tau_d$ , and  $\zeta$ , by  $\lambda = \mu\omega$ ,  $\tau_0 = \tau_d/\mu$ , and  $\zeta = \tau_d\omega$ . Then, from (4.10),  $\zeta$  is a root of

$$F(\zeta) \equiv \frac{\zeta}{\tau_d} - G(\zeta) = 0, \quad G(\zeta) \equiv \sqrt{1 + \zeta} \tanh \theta_0 \tanh \left[ \theta_0 \sqrt{1 + \zeta} \right] - 1. \quad (4.11)$$

By examining the roots of (4.11) in the complex  $\zeta$  plane, the following result was proved in §5 of [19].

**Proposition 4.1:** *There is a complex conjugate pair of pure imaginary eigenvalues to (4.10) at some unique value  $\tau_d = \tau_{dh}$  depending on  $D$ . For any  $\tau_d > \tau_{dh}$  there are exactly two eigenvalues in the right half-plane. These eigenvalues have nonzero imaginary parts when  $\tau_{dh} < \tau_d < \tau_{dm}$ , and they merge onto the positive real axis at  $\tau_d = \tau_{dm}$ . They remain on the positive real axis for all  $\tau_d > \tau_{dm}$ .*

The numerically computed Hopf bifurcation value  $\tau_{dh}$  is plotted versus  $D$  in Fig. 4(a). In Fig. 4(a) we also plot the magnitude  $|\omega_h|$  of the pure imaginary eigenvalues  $\omega_h = \pm i|\omega_h|$  at  $\tau_d = \tau_{dh}$ . Since  $\tau_0 = \tau_d/\mu$  and  $\tau = \varepsilon^{-2}\mathcal{A}^{-2}\tau_0$ , the Hopf bifurcation value for the onset of an oscillatory drift instability for a one-spike solution is

$$\tau_{tw} \sim \varepsilon^{-2}\mathcal{A}^{-2}\tau_{0d}, \quad \tau_{0d} \equiv \frac{\tau_{dh}}{\mu}, \quad \mu \equiv \frac{\theta_0}{6} \tanh \theta_0 \left[ 1 + \sqrt{1 - \frac{\mathcal{A}_{1e}^2}{\mathcal{A}^2}} \right]^2. \quad (4.12)$$

Recall from (3.22) that there is an oscillatory instability in the amplitude of an equilibrium spike when  $\tau = \tau_h = O(\mathcal{A}^4)$ . Thus,  $\tau_h \ll \tau_{tw}$  when  $O(1) \ll \mathcal{A} \ll O(\varepsilon^{-1/3})$  and  $\tau_{tw} \ll \tau_h$  when  $O(\varepsilon^{-1/3}) \ll \mathcal{A} \ll O(\varepsilon^{-1/2})$ . In Fig. 4(b) we plot  $\log_{10}(\tau_{tw})$  and  $\log_{10}(\tau_h)$  versus  $\mathcal{A}$ , showing the exchange in the dominant instability mechanism in the intermediate regime. For the equilibrium problem on the infinite line this exchange in the dominant instability mechanism was also noted in [21] and [4]. As a remark, we notice that  $\omega_h$ , representing the (scaled) temporal frequency of small oscillations, satisfies  $\omega_h \rightarrow 0$  in the infinitely long domain limit  $D \rightarrow 0$ . Therefore, the existence of an oscillatory instability requires a finite domain.

## 4.1 Numerical Solution of the Coupled ODE-PDE Stefan Problem

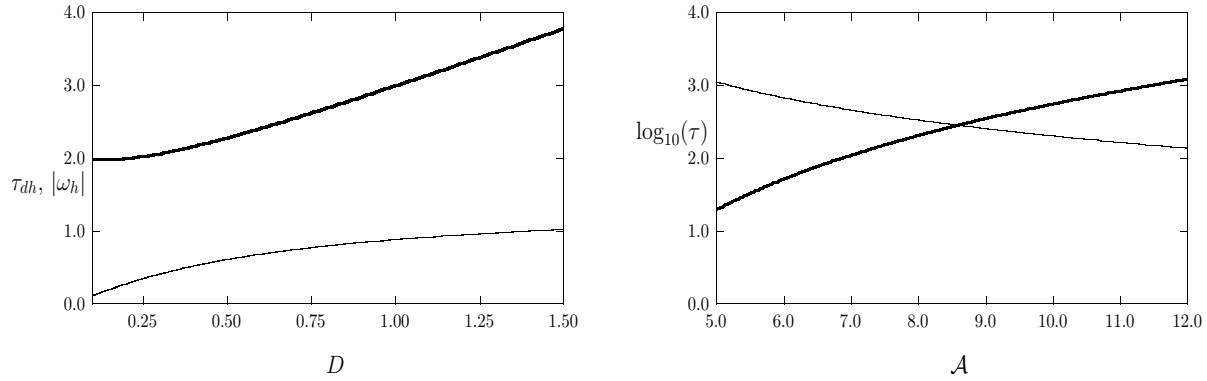
To compute numerical solutions to the Stefan problem (4.1) we adapt the numerical method of [32] for computing solutions to a heat equation with a moving singular Dirac source term. We use a Crank-Nicholson scheme to discretize (4.1a) together with a forward Euler scheme for the ODE (4.1b).

For simplicity we first consider (4.1a) for one spike where  $k = 1$ . Let  $h$  and  $\Delta t$  denote the space step and time step, respectively. We set  $\Delta t = h^2/2$  to satisfy the stability requirement of the forward Euler scheme. The number of grid points is  $M = 1 + 2/h$ , and we label the  $j^{\text{th}}$  grid point by  $x_j = -1 + (j - 1)h$  for  $j = 1, \dots, M$ . The total time period is  $T_m$ , and we label  $\sigma_n = n\Delta t$  for  $n = 1, \dots, T_m/\Delta t$ . At time  $\sigma_n$ , the solution  $u(x_j, \sigma_n)$  at the  $j^{\text{th}}$  grid point is approximated by  $U_j^n$ , and we label  $\mathbf{U}^n = (U_1^n, \dots, U_M^n)^T$ . Also, the spike location  $\xi_1(\sigma_n)$  and spike amplitude  $\gamma_1(\sigma_n)$  are approximated by  $\xi_1^n$  and  $\gamma_1^n$ , respectively.

As in [32] we approximate the delta function  $\delta(x - \xi_1)$  in (4.1a) with the discrete delta function  $d^{(1)}(x - \xi_1)$ , where  $d^{(1)}(y)$  is given by

$$d^{(1)}(y) = \begin{cases} (2h - |y|)/(4h^2), & |y| \leq 2h, \\ 0, & \text{otherwise.} \end{cases} \quad (4.13)$$

The numerical approximation  $d^{(1)}$  of the delta function in (4.1a) spreads the singular force to the neighboring grid points within its support. Next, we write the constraint of (4.1c), given by  $u(\xi_1(\sigma), \sigma) = 1/(\gamma_1\mathcal{A}^2)$ ,



(a)  $\tau_{dh}$  and  $|\omega_h|$  vs.  $D$

(b)  $\log_{10}(\tau_{tw})$  and  $\log_{10}(\tau_h)$  vs.  $\mathcal{A}$

Figure 4: Left Figure: The drift instability thresholds  $\tau_{dh}$  (heavy solid curve) and  $|\omega_h|$  (solid curve) versus  $D$ . Right figure: Plots of  $\log_{10}(\tau_h)$  (heavy solid curve) from (3.22) with  $k = 1$  and  $\log_{10}(\tau_{tw})$  (solid curve) from (4.12) versus  $\mathcal{A}$  for  $D = 0.75$  and  $\varepsilon = 0.015$ . This shows the exchange in the dominant instability mechanism in the intermediate regime.

in the form

$$u(\xi_1(\sigma), \sigma) = \int_{-\infty}^{\infty} u(x, \sigma) \delta(x - \xi_1(\sigma)) dx = \frac{1}{\gamma_1 \mathcal{A}^2}. \quad (4.14)$$

With  $U_j^n \approx u(x_j, \sigma_n)$ ,  $\xi_1^n \approx \xi_1(\sigma_n)$ , and  $\gamma_1^n \approx \gamma_1(\sigma_n)$ , the discrete version of (4.14) is

$$u(\xi_1^n, \sigma_n) \approx h \sum_j U_j^n d^{(2)}(x_j - \xi_1^n) = \frac{1}{\gamma_1^n \mathcal{A}^2}, \quad (4.15)$$

where  $d^{(2)}(y)$  is a further numerical approximation to the delta function given explicitly by

$$d^{(2)}(y) = \frac{1}{h} \begin{cases} 1 - (y/h)^2, & |y| \leq h, \\ 2 - 3|y|/h + (y/h)^2, & h \leq |y| \leq 2h, \\ 0, & \text{otherwise.} \end{cases} \quad (4.16)$$

The function  $d^{(2)}$  aims at interpolating grid values  $U_j^n$  to approximate the requirement  $u(\xi_1^n, \sigma_n) = 1/(\gamma_1^n \mathcal{A}^2)$  at the spike location.

A rough outline of the algorithm for the numerical solution to (4.1) to advance from the  $n^{\text{th}}$  to the  $(n+1)^{\text{th}}$  time-step is as follows:

1. Use (4.1b) to take a forward Euler step to get the new location  $\xi_1^{n+1}$  given  $\mathbf{U}^n$  and  $\gamma_1^n$ .
2. Use the approximate condition

$$u(\xi_1^{n+1}, \sigma_{n+1}) \approx \frac{1}{2\mathcal{A}^2} \left( \frac{1}{\gamma_1^n} + \frac{1}{\gamma_1^{n+1}} \right), \quad (4.17)$$

on the right hand-side of (4.15) together with the Crank-Nicholson discretization of (4.1a) to solve for  $\gamma_1^{n+1}$ .

3. Calculate  $\mathbf{U}^{n+1}$  from the discretization of (4.1a) using the value of  $\gamma_1^{n+1}$ .
4. Set  $n = n + 1$ , and repeat the iteration.

In order to obtain higher accuracy, we use a fourth order accurate scheme as suggested in [32] to approximate the second order differential operator  $u_{xx}$  as

$$u_{xx}(x_j, \sigma_n) \approx \begin{cases} (U_{j+4}^n - 6U_{j+3}^n + 14U_{j+2}^n - 4U_{j+1}^n - 15U_j^n + 10U_{j-1}^n)/(12h^2), & j = 1, \\ (-U_{j+2}^n + 16U_{j+1}^n - 30U_j^n + 16U_{j-1}^n - U_{j-2}^n)/(12h^2), & 2 \leq j \leq N, \\ (U_{j-4}^n - 6U_{j-3}^n + 14U_{j-2}^n - 4U_{j-1}^n - 15U_j^n + 10U_{j+1}^n)/(12h^2), & j = M, \end{cases}$$

where  $U_0^n$  and  $U_{M+1}^n$  are ghost points outside each end of the boundaries at  $x = \pm 1$ . The Neumann condition  $u_x(\pm 1, t) = 0$  is also discretized as

$$\begin{aligned} u_x(x_1, \sigma_n) &\approx (-3U_0^n - 10U_1^n + 18U_2^n - 6U_3^n + U_4^n)/(12h), \\ u_x(x_M, \sigma_n) &\approx (3U_{M+1}^n + 10U_M^n - 18U_{M-1}^n + 6U_{M-2}^n - U_{M-3}^n)/(12h). \end{aligned}$$

Eliminating the ghost points from the discretization of  $u_{xx}$ , we obtain the  $M \times M$  coefficient matrix

$$\mathbf{T} = \frac{1}{12h^2} \begin{pmatrix} -145/3 & 56 & -6 & -8/3 & 1 & 0 & 0 & 0 & \cdots & 0 \\ 58/3 & -36 & 18 & -4/3 & 0 & 0 & 0 & 0 & \cdots & 0 \\ -1 & 16 & -30 & 16 & -1 & 0 & 0 & 0 & \cdots & 0 \\ 0 & -1 & 16 & -30 & 16 & -1 & 0 & 0 & \cdots & 0 \\ 0 & 0 & -1 & 16 & -30 & 16 & -1 & 0 & \cdots & 0 \\ & & & \ddots & \ddots & \ddots & \ddots & \ddots & & \\ 0 & \cdots & 0 & 0 & -1 & 16 & -30 & 16 & -1 & 0 \\ 0 & \cdots & 0 & 0 & 0 & -1 & 16 & -30 & 16 & -1 \\ 0 & \cdots & 0 & 0 & 0 & 0 & -4/3 & 18 & -36 & 58/3 \\ 0 & \cdots & 0 & 0 & 0 & 1 & -8/3 & -6 & 56 & -145/3 \end{pmatrix}.$$

Next, we outline how we calculate the fluxes in (4.1b). For convenience, in the notation of this paragraph we omit the superscript  $n$  at time  $\sigma_n$ . In order to approximate the one-sided first order derivatives  $u_x(\xi_1^\pm, \sigma_n)$  in (4.1b), we first use the solution values at gridpoints on each side of  $\xi_1$  to interpolate the values at points that are equally distributed near  $\xi_1$ . Then, we approximate  $u_x(\xi_1^\pm, \sigma_n)$  by differencing values at these points. For instance, assuming that the closest grid point on the left-hand side of the spike is  $x_j$ , we use six point values  $(\bar{u}, U_j, U_{j-1}, U_{j-2}, U_{j-3}, U_{j-4})$  with  $\bar{u} = u(\xi_1, \sigma_n) = 1/(\gamma_1 \mathcal{A}^2)$  to interpolate the solution at  $x = (\xi_1 - 3h, \xi_1 - 2h, \xi_1 - h, \xi_1)$ . Denoting the results to be  $(U_1^-, U_2^-, U_3^-, U_4^-)$  with  $U_4^- = u(\xi_1, \sigma_n) = 1/(\gamma_1 \mathcal{A}^2)$ , we can use them for estimating  $u_x(\xi_1^-, \sigma_n)$  as

$$u_x(\xi_1^-, t) \approx (-3U_3^- + \frac{3}{2}U_2^- - \frac{1}{3}U_1^-)/h. \quad (4.18a)$$

Similarly, we obtain  $(U_1^+, U_2^+, U_3^+, U_4^+)$  at  $x = (\xi_1, \xi_1 + h, \xi_1 + 2h, \xi_1 + 3h)$  by interpolation, and we then discretize to obtain

$$u_x(\xi_1^+, t) \approx (3U_2^+ - \frac{3}{2}U_3^+ + \frac{1}{3}U_4^+)/h. \quad (4.18b)$$

Next, we discretize (4.1a) by the Crank-Nicholson scheme to get

$$\left[ \left(1 + \frac{1}{2}\mu\right)\mathbf{I} - \frac{\mu D}{2}\mathbf{T} \right] \mathbf{U}^{n+1} = \left[ \left(1 - \frac{1}{2}\mu\right)\mathbf{I} + \frac{\mu D}{2}\mathbf{T} \right] \mathbf{U}^n - 3\mu (\mathbf{d}^{n+1}\gamma_1^{n+1} + \mathbf{d}^n\gamma_1^n) + \mathbf{p}, \quad (4.19)$$

where  $\mu \equiv \Delta t/\tau_0$  and  $\mathbf{p}^t \equiv (\mu, \mu, \dots, \mu)$ . Here  $\mathbf{d}^{n+1}$  denotes the discretization of the delta function by  $d^{(1)}$  at time  $\sigma_{n+1}$ . Denoting the coefficient matrix of  $\mathbf{U}^{n+1}$  to be  $\mathbf{A}$  and that of  $\mathbf{U}^n$  to be  $\mathbf{B}$ , the system above can be written in the simpler form

$$\mathbf{A}\mathbf{U}^{n+1} = \mathbf{B}\mathbf{U}^n - 3\mu (\mathbf{d}^{n+1}\gamma_1^{n+1} + \mathbf{d}^n\gamma_1^n) + \mathbf{p}. \quad (4.20)$$

In (4.20), only the boldface variables are matrices and vectors. We then approximate (4.1c) by the discrete form (4.15). We write this interpolation as a dot product  $\mathbf{N}^{n+1}\mathbf{U}^{n+1}$ , where

$$\mathbf{N}^{n+1}\mathbf{U}^{n+1} = \frac{1}{2\mathcal{A}^2} \left( \frac{1}{\gamma_1^n} + \frac{1}{\gamma_1^{n+1}} \right). \quad (4.21)$$

Since  $\mathbf{A}$  is of full rank, we then left multiply (4.20) by  $\mathbf{N}^{n+1}\mathbf{A}^{-1}$  to get a quadratic equation for  $\gamma_1^{n+1}$  given by

$$3\mu\mathbf{N}^{n+1}\mathbf{A}^{-1}\mathbf{d}^{n+1}\gamma_1^{n+1} - \left[ \mathbf{N}^{n+1}\mathbf{A}^{-1}(\mathbf{B}\mathbf{U}^n - 3\mu\mathbf{d}^n\gamma_1^n + \mathbf{p}) - \frac{1}{2\mathcal{A}^2} \frac{1}{\gamma_1^n} \right] + \frac{1}{2\mathcal{A}^2} \frac{1}{\gamma_1^{n+1}} = 0. \quad (4.22)$$

Since  $\mathcal{A} \gg 1$ , we can solve (4.22) for the correct root  $\gamma_1^{n+1}$ . We then calculate  $\mathbf{U}^{n+1}$  using (4.20) and start the next iteration by using a forward Euler step on (4.1b) to advance the spike location.

This numerical method can be readily extended to treat (4.1) for two or more spikes. For instance, consider the case of two spikes. With the same Crank-Nicholson scheme, we let  $\mathbf{d}_1$  and  $\mathbf{d}_2$  be the discrete approximations of  $\delta(x - \xi_1)$  and  $\delta(x - \xi_2)$  in (4.1a), respectively, with the discrete delta function  $d^{(1)}$ . Define the row vectors  $\mathbf{N}_1^{n+1}$  and  $\mathbf{N}_2^{n+1}$  to the discrete versions of  $d^{(2)}$  near  $\xi_1$  and  $\xi_2$ , respectively. The conditions  $u(\xi_j^{n+1}, \sigma^{n+1}) = 1/(\gamma_j^{n+1}\mathcal{A}^2)$ , can then be approximated by the two discrete constraints

$$\mathbf{N}_j^{n+1}\mathbf{U}^{n+1} = \frac{1}{2\mathcal{A}^2} \left( \frac{1}{\gamma_j^n} + \frac{1}{\gamma_j^{n+1}} \right), \quad \text{for } j = 1, 2. \quad (4.23)$$

The Crank-Nicholson discretization of (4.1a) with  $k = 2$  is written as

$$\mathbf{A}\mathbf{U}^{n+1} = \mathbf{B}\mathbf{U}^n - 3\mu(\mathbf{d}_1^{n+1}\gamma_1^{n+1} + \mathbf{d}_2^{n+1}\gamma_2^{n+1}) - 3\mu(\mathbf{d}_1^n\gamma_1^n + \mathbf{d}_2^n\gamma_2^n) + \mathbf{p}. \quad (4.24)$$

Upon imposing the constraints (4.23) we obtain the following system for  $\gamma_1^{n+1}$  and  $\gamma_2^{n+1}$ :

$$\begin{aligned} & 3\mu\mathbf{N}_j^{n+1}\mathbf{A}^{-1}(\mathbf{d}_1^{n+1}\gamma_1^{n+1} + \mathbf{d}_2^{n+1}\gamma_2^{n+1}) + \frac{1}{2\mathcal{A}^2} \frac{1}{\gamma_j^{n+1}} \\ & - \left[ \mathbf{N}_j^{n+1}\mathbf{A}^{-1}(\mathbf{B}\mathbf{U}^n - 3\mu(\mathbf{d}_1^n\gamma_1^n + \mathbf{d}_2^n\gamma_2^n) + \mathbf{p}) - \frac{1}{2\mathcal{A}^2} \frac{1}{\gamma_j^n} \right] = 0, \quad \text{for } j = 1, 2. \end{aligned} \quad (4.25)$$

After calculating  $\gamma_1^{n+1}$  and  $\gamma_2^{n+1}$  from this system, we then compute  $\mathbf{U}^{n+1}$  from (4.25), and update the locations of the spikes.

## 4.2 Numerical Experiments of Oscillatory Drift Instabilities

We now perform some numerical experiments on (4.1) to verify the drift instability threshold of a one-spike solution given in (4.12). We also use the numerical scheme of §4.1 to compute large-scale oscillatory motion for some one and two-spike patterns.

For each of the numerical experiments below we give initial spike locations  $\xi_j(0) = \xi_{j0}$ , for  $j = 1, \dots, k$ , and we choose the initial condition  $u(x, 0)$  for (4.1) to be the quasi-equilibrium solution (2.14) with  $g_j = 1$  and  $x_j = \xi_{j0}$  for  $j = 1, \dots, k$  in (2.14). In all of the numerical computations below we chose the mesh size  $h = 0.01$  and the diffusivity  $D = 0.75$ . For  $D = 0.75$ , the stability threshold from Proposition 4.1 is computed numerically as  $\tau_{dh} = 2.617$ .

*Experiment 4.1: A one-spike solution near equilibrium: Testing the instability threshold*

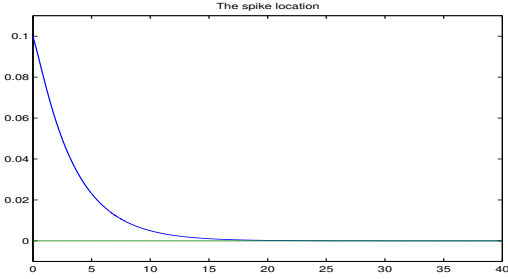
Let  $D = 0.75$  and  $\mathcal{A} = 28.5$ . Then, from (4.12) we calculate  $\tau_{0d} \approx 4.19$  and  $\tau_{tw} \approx 5177$ . For an initial spike location at  $\xi_1(0) = 0.1$ , in Fig 5 we plot the numerically computed spike layer trajectory  $\xi_1$  versus  $\sigma$  for six values of  $\tau_0$ . Comparing Fig. 5(d) with Fig. 5(e) we see that the amplitude of the oscillation grows slowly when  $\tau_0 = 4.22$ , and decays slowly when  $\tau_0 = 4.20$ . From Fig. 5(f) we observe that the drift Hopf bifurcation value is  $\tau_{0d} \approx 4.21$ , which compares favorably with the theoretical prediction of  $\tau_{0d} \approx 4.19$  from (4.12). With regards to the convergence of the numerical scheme for (4.1), we estimate numerically that  $\tau_{0d} \approx 4.23$  with the coarser meshsize  $h = 0.02$ , and that  $\tau_{0d} \approx 4.20$  for the very fine meshsize  $h = 0.005$ . As a trade-off between accuracy and computational expense, we chose  $h = 0.01$  in our computations.

*Experiment 4.2: A one-spike solution: Large-scale oscillatory dynamics*

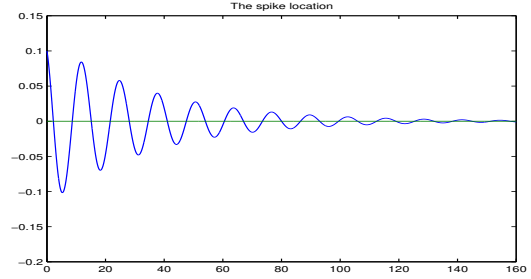
We again let  $D = 0.75$  and  $\mathcal{A} = 28.5$ . However, we now choose the initial spike location  $\xi_1(0) = 0.3$ , which is not near its equilibrium value. In Fig 6 we plot the numerically computed spike layer trajectory  $\xi_1$  versus  $\sigma$  for  $\tau_0 = 4.20$  and  $\tau_0 = 4.22$ . For the smaller value of  $\tau_0$  the spike slowly approaches its steady state at  $\xi_1 = 0$ . However, for  $\tau_0 = 4.22$ , the spike location exhibits a sustained large-scale oscillation.

*Experiment 4.3: A two-spike pattern: Oscillatory drift instabilities and the breather mode*

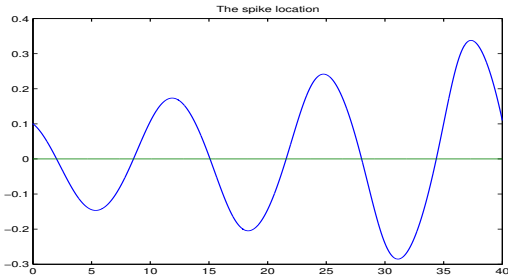
We now compute two-spike solutions. For  $D = 0.75$  and  $\mathcal{A} = 63.6$ , in Fig. 7(a) and Fig. 7(b) we plot the numerically computed spike trajectories with initial values  $\xi_1(0) = -0.38$  and  $\xi_2(0) = 0.42$  for two values of  $\tau_0$ . For  $\tau_0 = 16$  the spike trajectories develop a large-scale sustained oscillatory motion. In each case, the observed oscillation is of breather type, characterized by a  $180^\circ$  out of phase oscillation in the spike locations. A breather instability was shown in [11] to be the dominant instability mode for instabilities of equilibrium transition layer patterns for a Fitzhugh-Nagumo type model. It is also the dominant instability mode for equilibrium spike patterns of the GS model in the high-feed rate regime  $\mathcal{A} = O(\varepsilon^{-1/2})$  (see [18]). For the same values of  $D$  and  $\mathcal{A}$ , in Fig. 7(c) and Fig. 7(d) we plot the numerically computed spike trajectories with initial values  $\xi_1(0) = -0.55$  and  $\xi_2(0) = 0.45$  for  $\tau_0 = 15$  and  $\tau_0 = 17$ , respectively.



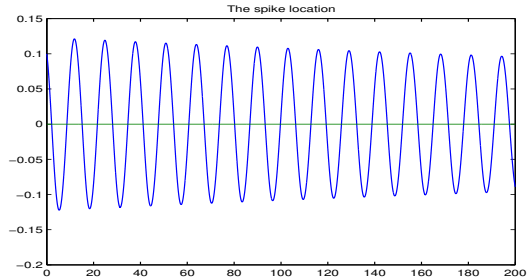
(a)  $\xi_1$  vs.  $\sigma$  for  $\tau_0 = 1.0$



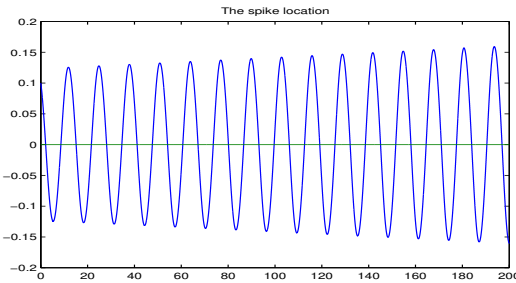
(b)  $\xi_1$  vs.  $\sigma$  for  $\tau_0 = 4.0$



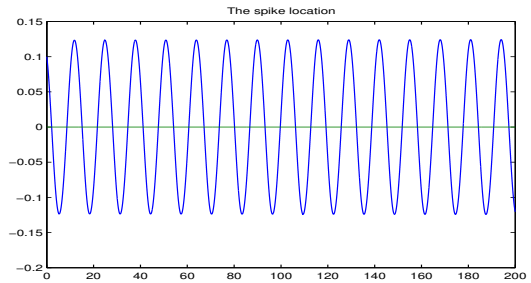
(c)  $\xi_1$  vs.  $\sigma$  for  $\tau_0 = 4.4$



(d)  $\xi_1$  vs.  $\sigma$  for  $\tau_0 = 4.20$

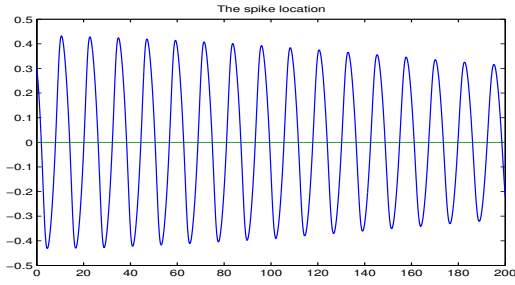


(e)  $\xi_1$  vs.  $\sigma$  for  $\tau_0 = 4.22$

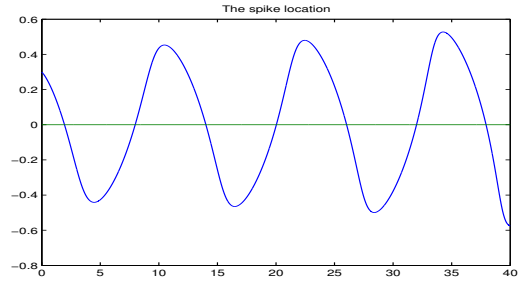


(f)  $\xi_1$  vs.  $\sigma$  for  $\tau_0 = 4.21$

Figure 5: *Experiment 4.1*: Testing the stability threshold for initial values near the equilibrium value. Plots of  $\xi_1$  versus  $\sigma$  with  $\xi_1(0) = 0.1$ ,  $D = 0.75$ , and  $\mathcal{A} = 28.5$ , for different values of  $\tau_0$ . The numerical threshold  $\tau_{0d} \approx 4.21$  in the plot in the lower right figure compares well with the theoretical prediction  $\tau_{0d} \approx 4.19$ .

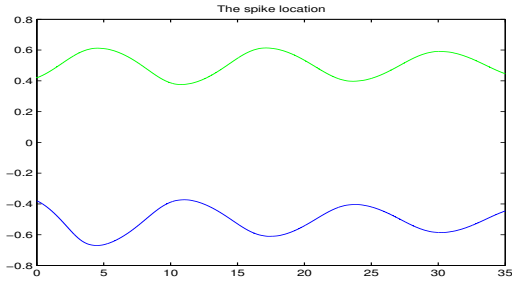


(a)  $\xi_1$  vs.  $\sigma$  for  $\tau_0 = 4.20$

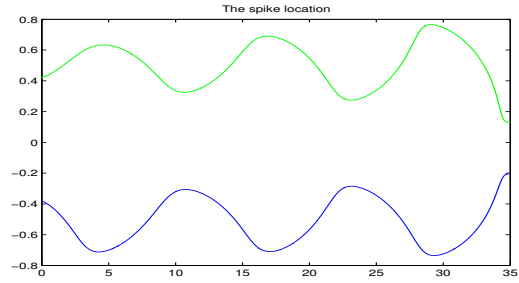


(b)  $\xi_1$  vs.  $\sigma$  for  $\tau_0 = 4.22$

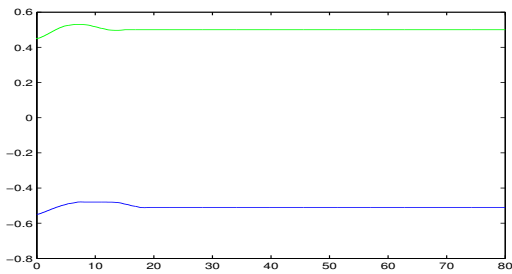
Figure 6: *Experiment 4.2*: Plots of  $\xi_1$  versus  $\sigma$  with  $\xi_1(0) = 0.3$ ,  $D = 0.75$ , and  $\mathcal{A} = 28.5$ . Left figure:  $\tau_0 = 4.20$ . Right figure:  $\tau_0 = 4.22$ .



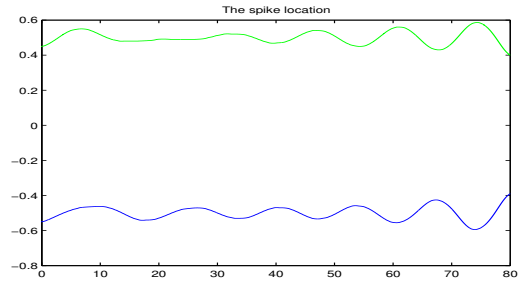
(a)  $\xi_j$  vs.  $\sigma$  for  $\tau_0 = 15$



(b)  $\xi_j$  vs.  $\sigma$  for  $\tau_0 = 16$



(c)  $\xi_j$  vs.  $\sigma$  for  $\tau_0 = 15$



(d)  $\xi_j$  vs.  $\sigma$  for  $\tau_0 = 17$

Figure 7: *Experiment 4.3*: Spike trajectories  $\xi_j$  versus  $\sigma$  for a two-spike pattern with  $D = 0.75$  and  $\mathcal{A} = 63.6$ . Top row: the initial values  $\xi_1(0) = -0.38$  and  $\xi_2(0) = 0.42$  with  $\tau_0 = 15$  and  $\tau_0 = 16$ . Bottom Row: the initial values  $\xi_1(0) = -0.55$  and  $\xi_2(0) = 0.45$  with  $\tau_0 = 15$  and  $\tau_0 = 17$ .



### 4.3 Integral Equation Formulation

In this section we show how to cast the Stefan problem (4.1) for a one-spike solution into an equivalent integral equation formulation. We let  $K(x, \sigma; \eta, s)$  to be the Green's function satisfying

$$\tau_0 K_\sigma = DK_{xx} - K + \delta(x - \eta)\delta(\sigma - s), \quad -1 < x < 1, \quad (4.26a)$$

$$K_x = 0 \quad x = \pm 1; \quad K = 0, \quad \text{for } 0 < \sigma < s. \quad (4.26b)$$

The solution to (4.26) can be represented either as an infinite sum of images, or else by an eigenfunction expansion. The latter representation is

$$K(x, \sigma; \eta, s) = \frac{H(\sigma - s)}{\tau_0} e^{-(\sigma - s)/\tau_0} \left[ \frac{1}{2} + \sum_{n=1}^{\infty} \exp\left(-\frac{Dn^2\pi^2(\sigma - s)}{4\tau_0}\right) \cos\left(\frac{n\pi}{2}(\xi + 1)\right) \cos\left(\frac{n\pi}{2}(\eta + 1)\right) \right]. \quad (4.27)$$

By using Green's identity, a straightforward calculation shows that the solution  $u(x, \sigma)$  to (4.1) with one spike can be written in integral form in terms of  $K$  as

$$u(x, \sigma) = 1 + \tau_0 \int_{-1}^1 [u(\eta, 0) - 1] K(x, \sigma; \eta, 0) d\eta - 6 \int_0^\sigma \gamma_1(s) K(x, \sigma; \xi_1(s), s) ds, \quad (4.28)$$

where  $\xi_1(s)$  is the spike trajectory. Imposing the constraint condition  $u = 1/(\gamma_1 \mathcal{A}^2)$  at  $x = \xi_1(\sigma)$ , we obtain an integral equation for  $\gamma_1(\sigma)$  in terms of the unknown spike location as

$$\frac{1}{\gamma_1(\sigma) \mathcal{A}^2} = 1 + \tau_0 \int_{-1}^1 [u(\eta, 0) - 1] K(\xi_1(\sigma), \sigma; \eta, 0) d\eta - 6 \int_0^\sigma \gamma_1(s) K(\xi_1(\sigma), \sigma; \xi_1(s), s) ds. \quad (4.29)$$

Finally, by calculating  $u_x$  as  $x \rightarrow \xi_1(\sigma)$  from above and from below, we calculate

$$u_x(\xi_1^\pm(\sigma), \sigma) = \tau_0 \int_{-1}^1 [u(\eta, 0) - 1] K_x(\xi_1^\pm(\sigma), \sigma; \eta, 0) d\eta - 6 \int_0^\sigma \gamma_1(s) K_x(\xi_1^\pm(\sigma), \sigma; \xi_1(s), s) ds. \quad (4.30)$$

Finally, by substituting (4.30) into (4.1c), we obtain the integrodifferential equation

$$\begin{aligned} \frac{d\xi_1}{d\sigma} = \gamma_1(\sigma) & \left( \tau_0 \int_{-1}^1 [u(\eta, 0) - 1] (K_x(\xi_1^+(\sigma), \sigma; \eta, 0) + K_x(\xi_1^-(\sigma), \sigma; \eta, 0)) d\eta \right. \\ & \left. - 6 \int_0^\sigma \gamma_1(s) (K_x(\xi_1^+(\sigma), \sigma; \xi_1(s), s) + K_x(\xi_1^-(\sigma), \sigma; \xi_1(s), s)) ds. \right) \end{aligned} \quad (4.31)$$

Here  $u(\eta, 0)$  is the initial condition for (4.1). This shows that the motion of the spike layer depends on its entire past history. This formulation shows that  $\xi_1(\sigma)$  is determined, essentially, by a continuously distributed delay model. Such problems typically lead to oscillatory behavior when  $\tau_0$  is large enough, this and suggests the oscillatory dynamics computed in §4.2.

We remark that as a result of the infinite image representation of  $K$ , together with the constraint (4.29), the integrodifferential equation (4.31) is significantly more complicated in form than a related integrodifferential equation studied numerically in [28] modeling a flame-front on the infinite line.

## 5 Discussion

We have studied the dynamics and oscillatory instabilities of spike solutions to the one-dimensional GS model (1.1) in the intermediate regime  $O(1) \ll \mathcal{A} \ll O(\varepsilon^{-1/2})$  of the feed-rate parameter  $\mathcal{A}$ . In the subregime  $O(1) \ll \mathcal{A} \ll O(\varepsilon^{-1/3})$ , and for  $\tau \ll O(\varepsilon^{-2}\mathcal{A}^2)$ , we have derived an explicit DAE system for the spike trajectories from the quasi-steady limit of the Stefan problem (2.13). From the analysis of a certain nonlocal eigenvalue problem, it was shown that the instantaneous spike pattern in this regime will become unstable to a Hopf bifurcation in the spike amplitudes at some critical value  $\tau = \tau_H = O(\mathcal{A}^4)$ . Alternatively, in the subregime  $O(\varepsilon^{-1/3}) \ll \mathcal{A} \ll O(\varepsilon^{-1/2})$ , and with  $\tau = O(\varepsilon^{-2}\mathcal{A}^{-2})$ , oscillatory drift instabilities for the spike locations were computed numerically from the full time-dependent Stefan problem (4.1) with moving sources. In this subregime, the onset of such drift instabilities occur at some critical value  $\tau = \tau_{TW} = O(\varepsilon^{-2}\mathcal{A}^{-2})$  that can be calculated analytically. An open technical problem is to study the codimension-two bifurcation problem that occurs when  $\mathcal{A} = O(\varepsilon^{-1/3})$  where both types of oscillatory instability can occur simultaneously at some critical value of  $\tau = O(\varepsilon^{-4/3})$ .

There are two key open problems that warrant further investigation. The first open problem is to extend the numerical approach of [28], used for a flame-front integrodifferential equation model, to compute long-time solutions to the integrodifferential equation formulation (4.31) of the Stefan problem (4.1). With such an approach, one could compute numerical solutions to (4.1) over very long time intervals to study whether irregular, or even chaotic, large-scale oscillatory drift behavior of the spike trajectories is possible for the GS model in the subregime  $O(\varepsilon^{-1/3}) \ll \mathcal{A} \ll O(\varepsilon^{-1/2})$ . A second key open problem is to systematically derive Stefan-type problems with moving sources from an asymptotic reduction of related reaction-diffusion systems with localized solutions such as the Gierer-Meinhardt model with saturation [15], the combustion-reaction model of [20], the Brusselator model of [16], and the GS model in two spatial dimensions. The derivation of such Stefan problems would allow for the study of large-scale drift instabilities of localized structures for parameter values far from their bifurcation values at which a normal form reduction, such as in [9] and [8], can be applied.

## References

- [1] R. P. Beyer, R. J. Leveque, *Analysis of a One-dimensional Model for the Immersed Boundary Method*, SIAM J. Numer. Anal., **29**, No. 2, (1992), pp. 332–364.
- [2] A. Doelman, W. Eckhaus, T. J. Kaper, *Slowly Modulated Two-Pulse Solutions in the Gray-Scott Model I: Asymptotic Construction and Stability*, SIAM J. Appl. Math., **61**, No. 3, (2000), pp. 1080–1102.
- [3] A. Doelman, W. Eckhaus, T. J. Kaper, *Slowly Modulated Two-Pulse Solutions in the Gray-Scott Model II: Geometric Theory, Bifurcations, and Splitting Dynamics*, SIAM J. Appl. Math., **61**, No. 6, (2000), pp. 2036–2061.
- [4] A. Doelman, R. A. Gardner, T. J. Kaper, *Stability Analysis of Singular Patterns in the 1D Gray-Scott Model: A Matched Asymptotics Approach*, Physica D, **122**, No. 1-4, (1998), pp. 1–36.

- [5] A. Doelman, R. A. Gardner, T. J. Kaper, *A Stability Index Analysis of 1D Patterns of the Gray-Scott Model*, Memoirs of the AMS, **155**, (2002).
- [6] A. Doelman, T. Kaper, *Semistrong Pulse Interactions in a Class of Coupled Reaction-Diffusion Equations*, SIAM J. Appl. Dyn. Sys., **2**, No. 1, (2003), pp. 53–96.
- [7] A. Doelman, T. Kaper, K. Promislow, *Nonlinear Asymptotic Stability of the Semi-Strong Pulse Dynamics in a Regularized Gierer-Meinhardt Model*, SIAM J. Math. Anal., **38**, No. 6, (2007), pp. 1760–1789.
- [8] S. Ei, *The Motion of Weakly Interacting Pulses in Reaction-Diffusion Systems*, J. Dynam. Differential Equations, **14**, No. 1, (2002), pp. 85–137.
- [9] S. Ei, H. Ikeda, *Dynamics of Front Solutions in Reaction-Diffusion Systems in One Dimension*, preprint, (2006).
- [10] M. Frankel, G. Kovacic, V. Roytburd, I. Timofeyev, *Finite-Dimensional Dynamical System Modeling Thermal Instabilities*, Physica D, **137**, No. 3-4, (2000), pp. 295–315.
- [11] T. Ikeda, Y. Nishiura, *Pattern Selection for Two Breathers*, SIAM J. Appl. Math., **54**, No. 1, (1994), pp. 195–230.
- [12] D. Iron, M. J. Ward, *The Dynamics of Multi-Spike Solutions to the One-Dimensional Gierer-Meinhardt Model*, SIAM J. Appl. Math., **62**, No. 6, (2002), pp. 1924–1951.
- [13] D. Iron, M. J. Ward, J. Wei, *The Stability of Spike Solutions to the One-Dimensional Gierer-Meinhardt Model*, Physica D, **150**, No. 1-2, (2001), pp. 25–62.
- [14] C. M. Kirk, W. E. Olmstead, *Blow-up Solutions of the Two-Dimensional Heat Equation due to a Localized Moving Source*, Anal. Appl. (Singap.), **3**, No. 1, (2005), pp. 1–16.
- [15] T. Kolokolnikov, W. Sun, M. J. Ward, J. Wei, *The Stability of a Stripe for the Gierer-Meinhardt Model and the Effect of Saturation*, SIAM J. Appl. Dyn. Sys., **5**, No. 2, (2006), pp. 313–363.
- [16] T. Kolokolnikov, T. Erneux, J. Wei, *Mesa-type Patterns in the One-Dimensional Brusselator and Their Stability*, Physica D, **214**, No. 1, (2006), pp. 63–77.
- [17] T. Kolokolnikov, M. Ward, J. Wei, *The Stability of Spike Equilibria in the One-Dimensional Gray-Scott Model: The Low Feed-Rate Regime*, Studies in Appl. Math., **115**, No. 1, (2005), pp. 21–71.
- [18] T. Kolokolnikov, M. Ward, J. Wei, *The Stability of Spike Equilibria in the One-Dimensional Gray-Scott Model: The Pulse-Splitting Regime*, Physica D, Vol. 202, No. 3-4, (2005), pp. 258–293.
- [19] T. Kolokolnikov, M. Ward, J. Wei, *Slow Translational Instabilities of Spike Patterns in the One-Dimensional Gray-Scott Model*, Interfaces Free Bound., **8**, No. 2, (2006), pp. 185–222.
- [20] M. Mimura, M. Nagayama, K. Sakamoto, *Pattern Dynamics in an Exothermic Reaction*, Physica D, **84**, No. 1-2, (1995), pp. 58–71.

- [21] C. Muratov, V. V. Osipov, *Traveling Spike Auto-Solitons in the Gray-Scott Model*, Physica D, **155**, No. 1-2, (2001), pp. 112–131.
- [22] C. Muratov, V. V. Osipov, *Stability of the Static Spike Autosolitons in the Gray-Scott Model*, SIAM J. Appl. Math., **62**, No. 5, (2002), pp. 1463–1487.
- [23] C. Muratov, V. V. Osipov, *Static Spike Autosolitons in the Gray-Scott Model*, J. Phys. A: Math Gen. **33**, (2000), pp. 8893–8916.
- [24] Y. Nishiura, H. Fujii, *Stability of Singularly Perturbed Solutions to Systems of Reaction-Diffusion Equations*, SIAM J. Math. Anal., **18**, (1987), pp. 1726–1770.
- [25] Y. Nishiura, H. Mimura, *Layer Oscillations in Reaction-Diffusion Systems*, SIAM J. Appl. Math., Vol. 49, No. 2, (1989), pp. 481–514.
- [26] Y. Nishiura, D. Ueyama, *A Skeleton Structure of Self-Replicating Dynamics*, Physica D, **130**, No. 1-2, (1999), pp. 73–104.
- [27] Y. Nishiura, D. Ueyama, *Spatio-Temporal Chaos for the Gray-Scott Model*, Physica D, **150**, No. 3-4, (2001), pp. 137–162.
- [28] J. H. Park, A. Bayliss, B. J. Matkowsky, A. A. Nepomnyashchy, *On the Route to Extinction in Nonadiabatic Solid Flames*, SIAM J. Appl. Math., **66**, No. 3, (2006), pp. 873–895.
- [29] J. E. Pearson, *Complex Patterns in a Simple System*, Science, **216**, (1993), pp. 189–192.
- [30] W. N. Reynolds, S. Ponce-Dawson, J. E. Pearson, *Dynamics of Self-Replicating Spots in Reaction-Diffusion Systems*, Phys. Rev. E, **56**, No. 1, (1997), pp. 185–198.
- [31] W. Sun, M. J. Ward, R. Russell, *The Slow Dynamics of Two-Spike Solutions for the Gray-Scott and Gierer-Meinhardt Systems: Competition and Oscillatory Instabilities*, SIAM J. App. Dyn. Systems, **4**, No. 4, (2005), pp. 904–953.
- [32] A. K. Tornberg, B. Engquist, *Numerical Approximations of Singular Source Terms in Differential Equations*, J. Comput. Phys., **200**, No. 2, (2004), pp. 462–488.
- [33] D. Ueyama, *Dynamics of Self-Replicating Patterns in the One-Dimensional Gray-Scott Model*, Hokkaido Math J., **28**, No. 1, (1999), pp. 175–210.
- [34] M. J. Ward, J. Wei, *Hopf Bifurcations and Oscillatory Instabilities of Spike Solutions for the One-Dimensional Gierer-Meinhardt Model*, Journal of Nonlinear Science, **13**, No. 2, (2003), pp. 209–264.
- [35] J. Wei, *On Single Interior Spike Solutions for the Gierer-Meinhardt System: Uniqueness and Stability Estimates*, Europ. J. Appl. Math., Vol. 10, No. 4, (1999), pp. 353–378.